Ocean Dynamics (2021) 71:357–378
https://doi.org/10.1007/s10236-020-01433-w

WAVERYS: a CMEMS global wave reanalysis during the altimetry period

Stéphane Law-Chune[1] · Lotfi Aouf[2] · Alice Dalphinet[2] · Bruno Levier[1] · Yann Drillet[1] · Marie Drevillon[1]

Received: 24 June 2020 / Accepted: 17 December 2020 / Published online: 30 January 2021

Abstract
As part of the Copernicus Marine Service, WAVERYS is the multi-year wave reanalysis that provides global wave data with a fine grid resolution of 1/5°. This wave reanalysis covers the period 1993–2019 and disseminates 3-h integrated wave parameters describing the sea state at the ocean surface. The wave model used is the version 4 of the model MFWAM, which is driven by sea ice fraction and wind provided by the atmospheric reanalysis ERA5. The WAVERYS includes the assimilation of altimeter wave data and directional wave spectra provided by Sentinel-1. The wave reanalysis includes also wave-current interactions by using 3-h surface current forcing provided by the ocean reanalysis GLORYS. This paper highlights the assessment of wave parameters provided by the WAVERYS. The validation has been performed with independent altimeter significant wave heights and buoy wave data. The results show the good accuracy of scatter index of SWH (significant wave height) which is 8.7% in comparison with HY-2A altimeter. Moreover, we point out that scatter index of SWH from the WAVERYS is improved by about 9% with respect to the ERA5 wave dataset. We also indicate the good accuracy of swell propagation thanks to the assimilation of directional wave spectra. An analysis has been conducted for wave-current interactions and also discussions about extreme values and trend of time series are suggested.

Keywords Wave reanalysis · Wave hindcast · Global wave modelling · Wave climate · MFWAM, CMEMS, wave spectra assimilation, wave-current interactions

1 Introduction

The Copernicus Marine Environment Monitoring Service (CMEMS) is a free and open-access European service whose mission is to provide scientifically qualified and systematic information on the physical and biogeochemical state of the oceans. One aspect of the service is the dissemination of ocean products derived from in situ and satellite observations or numerical models (see http://marine.copernicus.eu/). These products cover, for the global ocean and European regional seas, forecasts and analyses in real time as well as multi-year products (MYP). These latter are generally called reanalysis in case of data-assimilated models, or simply hindcasts when deprived of assimilation system. The use of models is particularly relevant for waves, as in situ observations provide scarce and inadequate spatial coverage and satellite observations has low temporal resolution with failures for near-shore and high latitude.

Learning from historical sea states is crucial for various ranges of activities that are at the heart of CMEMS benefits. Spatial distribution of waves allows the drawing of safer, eco-efficient shipping routes (Cavaleri et al. 2012; Roh 2013). The knowledge of extreme sea states and their occurrence are critical for dimensioning off shore structures and maritime vessels (Sarpkaya 2012; Szelangiewicz et al. 2014; Barbariol et al. 2019).The wave energy potential is another interesting resource for sustainable, clean energy development, and wave hindcasts may help to determine the best possible exploitation sites (Gunn and Stock-Williams 2012). Ocean waves also act on living organisms and biogeochemical resources in the surface layer through turbulence and transport wave-related processes (Chatelain and Guizien 2010; Röhrs et al. 2014),

Responsible Editor: Val Swail

This article is part of the Topical Collection on the *16th International Workshop on Wave Hindcasting and Forecasting in Melbourne, AU, November 10–15, 2019*

✉ Stéphane Law-Chune
stephane.lawchune@mercator-ocean.fr

[1] Mercator Ocean International, 10 Rue Hermès, 31520 Ramonville-Saint-Agne, France

[2] Météo France, 42 Avenue Gaspard Coriolis, 31100 Toulouse, France

making them relevant for monitoring and managing marine habitats and aquaculture. Moreover, long past series allow us to understand the role of waves in global climate variability, which eventually leads to more realistic scenarios within the climate projection framework (Lemos et al. 2019), and eventually a better coastal management for the near future.

Wave climatology efforts have been proposed from the 2000s onwards. Since the quality of wind forcing is critical for modelling waves (Durrant et al. 2013; Stopa 2018), the availability of a new state-of-the-art atmospheric reanalysis often makes the production of a wave reanalysis attractive. We can cite among them the ones carried out by the European Centre for Medium Range Weather Forecasts (ECMWF) with the ECWAM third-generation wave model (Hasselmann et al. 1988; Bidlot et al. 2007) coupled within their Integrated Forecasting System (IFS), like the 1.5° ERA40 reanalysis (Uppala et al. 2005), the 1° ERA-Interim reanalysis (Dee et al. 2011), and more recently the 0.5° ERA5 reanalysis (Hersbach et al. 2020). The WAVEWATCH3 model (Vinet and Zhedanov 2011) was also used to produces several global wave hindcasts, like the latest ones from the NCEP/NOOA reanalysis project (Chawla et al. 2013) forced by the CFSR atmospheric reanalysis (Saha et al. 2010), and from the Japan Meteorological Agency (Mori et al. 2017), driven by the JRA-55 atmospheric reanalysis (Kobayashi et al. 2015).

These wave reanalysis often exhibit strengths, weakness, and differences, notably on variability and extreme aspects, as shown by Caires et al. (2004) in their intercomparison exercise. The authors identified notably the Tropics and the Southern Ocean as problematic areas due to poor physical process knowledge and lack of available data. Global wave reanalyses are generally well-suited in describing the open ocean, but generally fail at the coast, often due to a lack of resolution. This lack of resolution affects both the representation of coastal winds and wave processes such as bottom friction, wave breaking, island shadowing, and fetch length. An approach proposed by the GOW2 reanalysis of Perez et al. (2017) to overcome this difficulty is to use a refined multi-scale grid at the coast and in the Southern Hemisphere for better interaction with ice. Another failure pointed out by Mínguez et al. (2012) concerns the representation of cyclones and their effects, which is very limited due to the coarseness of the spatiotemporal resolution used for the global models. Being nevertheless of secondary importance compared to the accuracy of atmospheric forcing and bathymetry, the refraction effects on waves due to large-scale currents are well-known (e.g. Irvine and Tilley 1988 for the Agulhas current, and Mapp et al. 1985 for the Gulf Stream). Ardhuin et al. (2017) have demonstrated the action of currents on wave fields at scales smaller than 100 km, with an amplification of the extreme events crossing small current structures. The use of surface currents affects the waves at the sea surface which, in turn, impact the atmospheric boundary layer and thus improves the estimate of winds.

This paper focuses on the first 1/5° global wave reanalysis produced by CMEMS which is called WAVERYS (WAVeReanalYSis). The WAVERYS is driven by the ERA5 10-m wind and sea ice fraction, as well as GLORYS12 oceanic currents (Lellouche et al. 2018). The period covered is the 1993 to-present altimetry period, which allows for the reanalysis system to assimilate data from past satellite missions, starting from Topex-Poseidon until Sentinel-3A mission. To better describe the propagation of swell wave systems, the WAVERYS assimilate directional wave spectra from synthetic aperture radar (SAR) provided by Sentinel-1A and -1B satellite missions. The WAVERYS v1.0 has been disseminated since December 2019, but this paper uses the version v1.1 that corrects some issues related to data assimilation (see Law-Chune et al. 2019).

The paper is organized as follows. Section 1 describes the WAVERYS model configuration, its set-up and the selected input data. Section 2 concerns the validation of integrated wave parameters. This has been performed using SWH (significant wave height) from HY-2A satellite and also buoys data in deep ocean and coastal areas. Section 3 presents the impact of wave-current interactions on mean parameters, as well as extreme value and trends for mean parameters.

2 System description

2.1 Wave model and set-up

The wave reanalysis is performed with the MFWAM wave model updated for CMEMS global system in 2018, namely MFAM V4. MFWAM is based on ECWAM computing code IFS-38R2 (ECMWF 2012) with different source terms related to dissipation by wave breaking and swell damping induced by air friction at the sea surface. The dissipation by white-capping used in MFWAM is ST4-like as described in Ardhuin et al. (2010). The model has been upgraded with adjustments of the dissipation source term and also improvement on drag coefficient by using a Philips spectrum tail for high-frequency waves. The setting parameters of the dissipation terms are given in Table 2 in appendix. The non-linear source term uses the DIA approach developed by Hasselmann and Hasselmann (1985). The wind input term is based on the source term given by Bidlot et al. (2007) modified by a sheltering effect for short waves and negative input term of swell damping induced by air-sea friction (Ardhuin et al. 2010). The model MFWAM is set with reduced latitude-longitude grid and includes island obstructions scheme which induces a better wave propagation around islands, mostly in the Pacific Ocean.

The bathymetry is generated by using 2-min gridded global topography data from ETOPO2/NOAA (National Geophysical Data Center 2006). The native model grid has equal spacing of 1/5° between latitudes. Along the equator, the distance is fixed with grid size 1/5° and the number of points on each latitude towards the poles is reduced to maintain as much as possible an equal physical distance between them (Bidlot 2012a). The wave spectrum is discretized in 24 directions and 30 frequencies starting from 0.035 up to 0.58 Hz. A minimum water depth is set at 5 m, which is more than sufficient at the 1/5° global resolution to represent shoaling effects.

2.2 Winds

The WAVERYS is forced by 10-m wind and sea ice fraction provided by the ERA5 climate reanalysis produced at the ECMWF (Hersbach et al. 2020). These data were obtained from the MARS archive with an average native resolution of 31 km and have been interpolated to fit the wave model grid size of 0.2°. Besides, although hourly analysis fields are available, a 3-h forcing has been selected for consistency with surface current forcing and data assimilation window. It has been demonstrated that the ERA5 has improved the quality of winds by 20% in comparison with ERA-Interim. Belmonte Rivas and Stoffelen (2019) also showed that the ERA5 performance is close to current operational IFS-ECMWF forecasts.

2.3 Assimilation system

The assimilation system implemented in the MFWAM model jointly uses SWH provided by altimeter missions and the directional wave spectra from Sentinel-1 mission through the synthetic aperture radar (SAR). The first part of the assimilation consists in performing an optimal interpolation of SWH as developed by Lionello et al. (1992) with a distance of influence of the observation up to 600 km. The assimilation is performed sequentially every 3 h, and there is no correction applied for the wind input. The model and observation errors are considered equal for the optimal interpolation. Then, a scaled analyzed wave spectrum in frequency range is carried out by using empirical growth laws depending on the wave physics of the model (Lionello et al. 1992). As this is derived from wind wave growth power law relation, this correction affects more the wind sea part of the spectrum than the swell.

The second part of the assimilation system consists in the assimilation of SAR wave spectra, which is implemented following several procedures. The first procedure performs a partitioning principle to split the first guess and observes wave spectrum into several partitions or dominant wave trains. Then, the mean energy and the two-wave number components of each partition are computed, and a cross assignment between observed and modelled wave partitions is performed. This cross-association consists in selecting observed and modelled wave partitions which are close to each other depending on a threshold normalized distance of the components of wave number, as developed in Aouf et al. (2006, 2016). Afterwards, an optimal interpolation is applied to mean energy and wave number components of the associated partitions. Finally, an analyzed wave spectrum is reconstructed by superposing the analyzed partitions while respecting the validity of frequency cut-off for SAR wave spectra. A bilinear interpolation between analyzed partitions is also applied to avoid incoherent gaps in the analyzed spectrum.

2.3.1 Altimeter data

The assimilation of altimetry data allows to significantly improve short-term forecasts (Abdalla and Janssen 2017) and the WAVERYS takes advantage of most of historical altimeter wave data. Appendix 2 provides additional information on their spatial and temporal coverage. The altimeter wave data have been reprocessed by CERSAT-IFREMER (Queffeulou and Croizé-Fillon 2016) in the frame of GlobWave project supported by the European Space Agency. The assimilation of SWH is performed over the entire period with a time step and a centred assimilation window of 3 h.

2.3.2 Wave spectrum data

Since the EnviSat satellite mission, it has been demonstrated that the SAR detects accurately wave spectra related to swell systems with wavelength on average greater than 200 m (Hasselmann et al. 2013). This cut-off related to wavelength is variable and depends on the satellite along track and the wave directions. In the WAVERYS, we used SAR wave spectra, which are provided by European Space Agency (ESA) in the frame of Sentinel-1 (S1) missions, supported by the Copernicus space program. Two satellites S1A and S1B are currently flying and providing level 2 SAR wave products. The SAR directional wave spectra are processed by instrument processing facility (IPF) versions 2.8 and 3.0 which is upgraded with significant improvement in capturing wave systems (Hajduch et al. 2020). The wave spectra from S1A starts from March 2016, while those from S1B satellite starts from August 2018. The level 2 SAR wave spectra from S1 has been improved with an upgraded processing which gives better flags to remove corrupted data. A quality control procedure for SAR wave spectra has been implemented by considering thresholds on retrieved SAR wind speed, normalized variance of images, and signal to noise ratio. We also used the variable wavelength cut-off provided in the level 2 products. Figure 1 shows a polar plot of SAR wave spectrum on 14 May 2018 at 6:00 (UTC). We can see clearly at least 3 wave systems with a strong swell propagating to the north-east direction.

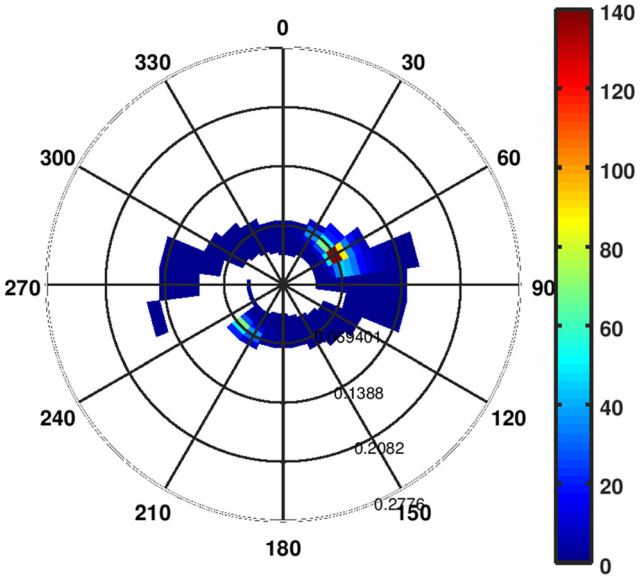

Fig. 1 Sentinel-1A SAR directional wave spectrum at position with longitude of 198.2° W and latitude of 42° S on 14 May 2018 at 06:00 (UTC). The colourbar indicates the density of energy (m^2/Hz/°) in frequency and direction. Directions are in the oceanographic convention (direction towards)

Such wave partitions are assimilated to correct the uncertainties of low-frequency part of the wave spectrum computed from the wave model. The WAVERYS is the first available global wave reanalysis that assimilates SAR wave spectra measured from space. The assimilation of these data makes it possible to very effectively control long swells, typically those generated in the Southern Ocean (Aouf et al. 2018; Le Traon et al. 2019).

2.4 Ocean currents

Any horizontal current shear involves wave refraction and modification of wave frequencies according to the laws of optics and Doppler effect. In the case of upstream flow relative to the direction of the waves, the breaking or reflection of wave trains can even occur (ECMWF 2012). To provide the most realistic and accurate sea state, the WAVERYS takes into account 3-h surface currents provided by the global physical reanalysis of CMEMS, namely GLORYS12V1 (Drévillon et al. 2018). GLORYS12 currents are interpolated on the 1/5° native grid of the wave model. Taking into account ocean currents has shown very positive results for wave fields interacting with high-energy current systems such as the Agulhas currents (Aouf et al. 2019).

2.5 Output parameters

The WAVERYS provides users with 17 integrated wave parameters describing sea state such as SWH, mean and peak wave periods, and dominant wave direction. The wave reanalysis includes the partitioning on wave spectra and provides also mean parameters for wind-sea and primary and secondary swell wave systems. Directional wave spectra are saved only on a very limited number of points of the domain for validation purpose and not distributed because of the large volume of data they generate. The WAVERYS also provides boundary conditions for regional CMEMS wave reanalysis such as IBI and Mediterranean domains.

3 Validation

Statistical parameters on the difference between observed (Obs) and reanalyzed (Model) wave variables were computed with the following definitions:

- Average differences or bias:

$$\text{bias} = \overline{\text{Model}(t) - \text{Obs}(t)}$$

- Root mean squared deviation (RMSD):

$$\text{RMSD} = \sqrt{\overline{(\text{Model}(t) - \text{Obs}(t))^2}}$$

- Scatter index (SI):

$$\text{SI} = \frac{\sqrt{\overline{\left(\left(\text{Model}(t) - \overline{\text{Model}(t)}\right) - \text{Obs}(t) - \overline{\text{Obs}(t)}\right)^2}}}{\overline{\text{Obs}(t)}}$$

- HH index: Mentaschi et al. (2013) highlighted some concerns with RMSE-derived metrics that favour negatively biased models. These authors suggest the use of the unbiased HH metric:

$$\text{HH} = \frac{\sqrt{\overline{\left((\text{Model}(t) - \text{Obs}(t)\right)^2}}}{\overline{\text{Model}(t).\text{Obs}(t)}}$$

We will use from time to time this diagnostic, although we will favour more the SI because of its widespread use that allows for a direct comparison with other studies.

3.1 Open Ocean validation

3.1.1 Comparison with altimeter HY-2A

The HY-2A satellite of the Haiyang series is China's first ocean dynamic environment satellite. The HY-2A is equipped with an altimeter which provides SWH every 7 km on ground tracks. As the HY-2A is not assimilated in the WAVERYS, it is then well-suited for the validation of SWH. Level 2 wave

data from the HY-2A have been processed by the French Space Agency CNES. The data have been downloaded from AVISO+ web portal. A quality control based on thresholds for backscattered signal section (σ0), SWH, and standard deviation of SWH has been applied for the HY-2A level 2 data. By using the ocean flag provided in the level 2 data, SWH from the HY-2A covers all ocean basins and gets close to the coast line until 7 km.

3.2 Method

SWH from H2A was first recalibrated with respect to Jason-2, one of the most stable altimetry missions (see Appendix 3). Validation with altimeter HY-2A was performed globally on a grid size of 0.5° and a time window of 3 h. The procedure consists in computing super-observations by averaging SWH of the HY-2A in a box of 0.5° grid size and considering the nearest SWH from the WAVERYS. The validation period starts from January 01, 2014, until December 26, 2018. SWH outside the range [0.5–16] m are discarded to avoid corrupted data in the analysis; the same is done for model equivalents.

3.3 Comparison to ERA5 wave dataset

As the HY-2A is not used in the assimilation of the ERA5 wave reanalysis, this is a good opportunity to check the performance of both wave reanalysis in terms of analyzed SWH.

The ERA5 is a coupled system forced with 10-m neutral winds to which are added effect of turbulence related to wind gust and atmospheric boundary layer stability (ECMWF 2015). However, the winds seen by the two systems should be relatively similar. The two systems are more differentiated by their grid resolution and wave physics. The ERA5 has a coarser grid resolution of 0.5°, while the WAVERYS has a finer grid size of 0.2°. The WAVERYS includes wave-current interactions but without any coupling with an atmospheric model like ERA5. The two-wave reanalysis systems are also quite different in terms of dissipation by white-capping terms. The WAVERYS is based on ST4-like physics while the ERA5 uses ECWAM-IFS41R2 physics developed from Bidlot et al. (2007). It is admitted that this latter is less skilled for swell propagation.

4 Results

Figure 2 shows scatter plots of SWH from the two-wave reanalysis (WAVERYS and ERA5) and the altimeter HY-2A during the period 2014 to 2018. The linear regression shows a better slope of 0.97 for the WAVERYS in comparison with 0.93 for ERA5. This is explained in particular for the high order quantiles (higher than 95th for heights above 6.5 m) which are underestimated in the ERA5 compared to the HY-2A. The good agreement up to the 99.9th percentile between the observation and WAVERYS shows the good accuracy of SWH that can lead to better analysis for studies related to climate averages and statistical distributions in open ocean. The series being arranged in chronological order along the altimeter tracks, the very high correlation of 0.98, show that the wave reanalysis reproduced in a very realistic way the different wave systems encountered following the satellite tracks. The bias of SWH is reasonably small, less than 5 cm, which is for instance less than 5% for SWH range of 1 m. The WAVERYS shows a global positive bias of SWH of 4 cm and a root mean square error (RMSE) of difference of 22 cm, whereas the ERA5 indicates a zero overall bias and an RMSE of 24 cm. The scatter index (SI) of SWH gives the dispersion between model and altimeter data. We found remarkably a better SI of SWH for the WAVERYS of 8.66% in comparison with 9.55% for ERA5. Considering all the points of the series, the improvement of the WAVERYS compared to the ERA5 is equal to 9.3% in terms of SI and 9% in terms of HH.

A kernel density Gaussian estimator was applied to the SWH series to estimate its probability density function (PDF) of SWH. The left side of Fig. 3 shows these PDF estimates for the two-wave reanalysis and the altimeter HY-2A. The PDFs of the models fit well with the one from the altimeter HY-2A, except in the SWH range of 1.75–2.50 m where models are overpopulated compared the satellite data. These height ranges correspond to those most frequently encountered waves in the global domain, with occurrences around 45% for the HY-2A, 48% for the WAVERYS, and 50% for the ERA5. In this range of SWH, we can easily see that WAVERYS pdf is closer to the one of the altimeter HY-2A. It can also be noted that waves between 0.5 and 1 m have a higher population in the HY-2A than in the models. For example, waves of about 0.75 m represent 10% of the population in the observations, whereas they represent only 5% of the population in the models. The difference in density for small waves can be explained by a lack of resolution and realism in the wind forcing for small scales (1/4° of resolution), but also by the limitation of growth and conservation of these short scales in the wave model physics, all the more so with meshes of resolution no more precise than 1/5°. It is also worthy to mention the increase of uncertainties of retrieval for small SWH (< 1 m) for satellite altimetry.

The right panel of Fig. 3 shows the cumulative distribution of normalized bias, SI, and HH index for the WAVERYS with respect to the HY-2A. It can be seen, for example, that 80% of the WAVERYS domain has an SI and normalized bias of less than 10% and 3%, respectively. The median value of the WAVERYS domain is less than 7% for SI, and only 10% of the domain has SI values below 4%.

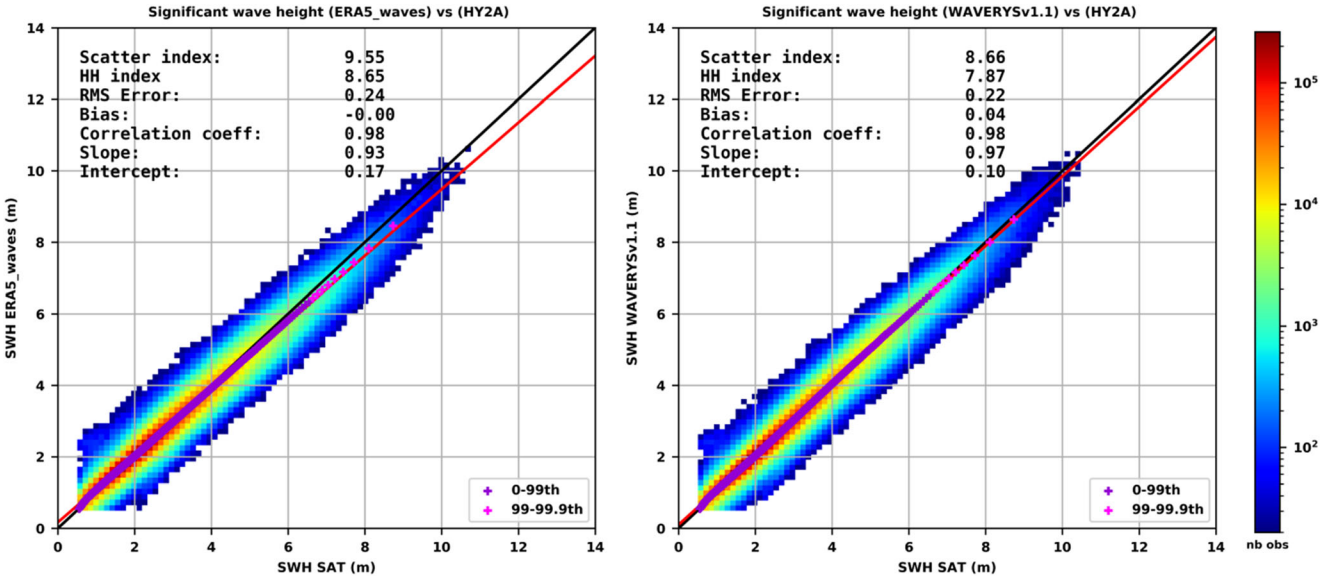

Fig. 2 Scatter plots of SWH from altimeter HY-2A and the models (left panel for ERA5 and right panel for WAVERYS). The colourbar represents the density of points. Statistical parameters are given, as well as the slope and intercept associated with the linear regression. Cross marks represent quantiles vs. quantiles values, and the pink ones refer to highest quantiles (99–99.9th percentiles)

Figure 4 presents global bias and SI maps for SWH obtained by the WAVERYS and ERA5. In the following, only data between latitudes 70° S and 80° N have been kept, in order to remove uncertainties related to points affected by the sea ice as obtained from the ERA5 (Hersbach et al. 2020). The remaining Polar Regions are those where the bias of SWH reaches roughly 80 cm as illustrated in Fig. 4. Other ocean regions show a bias of SWH about 20–40 cm, like the inner seas and complex coastal areas. This is mainly because of uncertainties related to the wind forcing and lack of coastal grid resolution in the wave models. Interestingly, the southern mid-latitude band (30° S–60° S) and the North Atlantic are low biased of roughly − 10 cm for the ERA5, which explains an overall zero bias in Fig. 2, due to latitude compensation for bias. However, the WAVERYS shows a better feature with a small slightly positive bias of SWH for these areas. The average SWH bias of the WAVERYS remains below 10 cm overall, except in the storm track zone where it can reach 15 cm, likely related to strong wind conditions.

SI maps for SWH clearly show that coastal regions record the highest values ranging between 16 and 20%. We can also remark that for closed seas such as the Mediterranean Sea, Japan, and Java Sea where the winds can change rapidly, the SI of SWH remains reasonable with range between 12 and 15%.

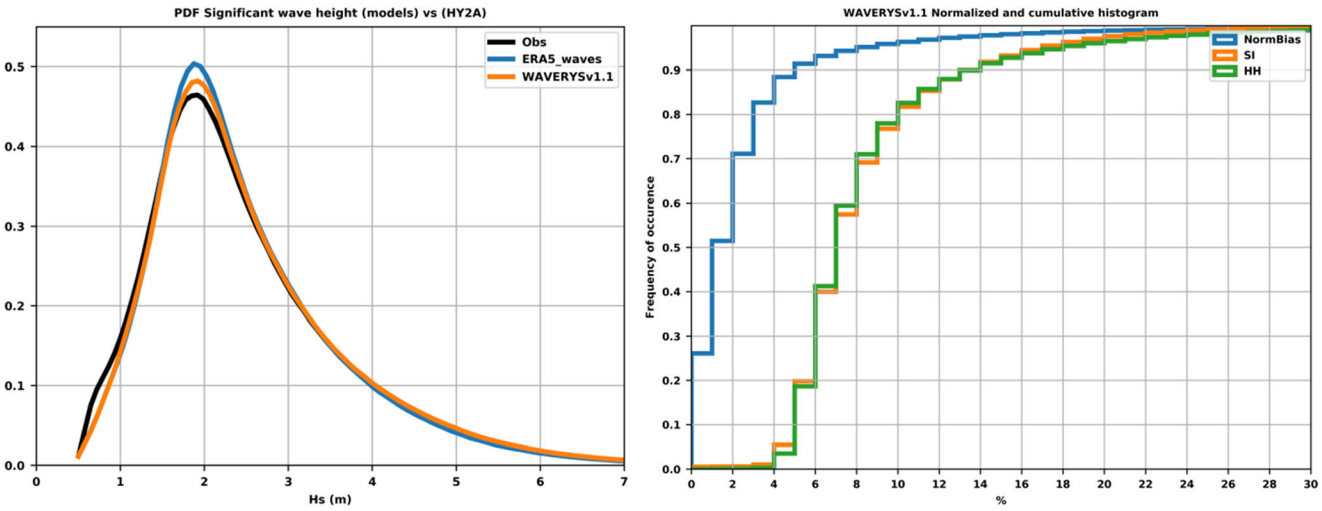

Fig. 3 Left panel shows the probability density function for SWH from HY-2A, ERA5, and WAVERYS. Right panel displays the normalized and cumulative histograms of the mean scatter index and the mean normalized bias over the total domain for WAVERYS (mean considered values are temporal averages all over the time series)

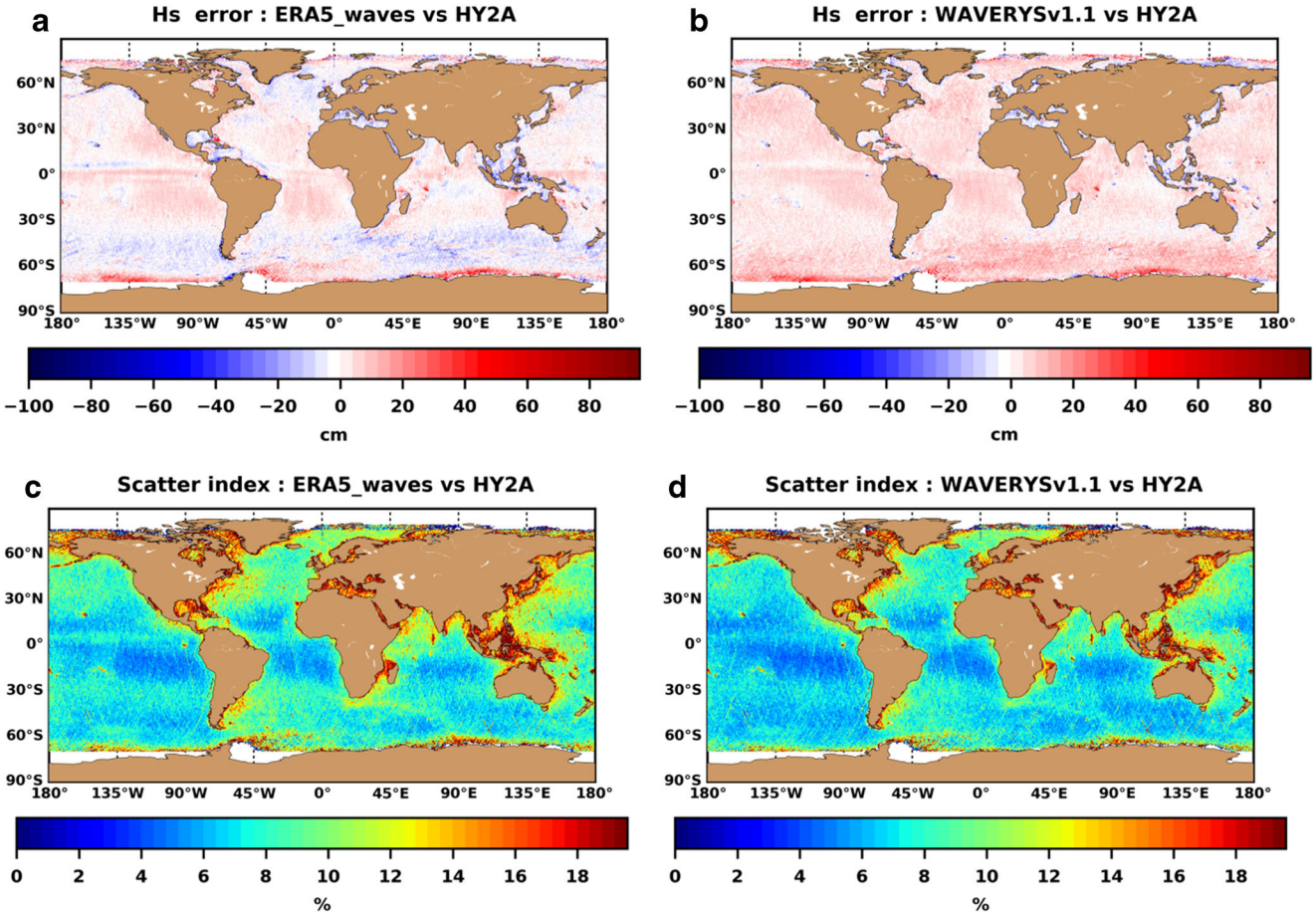

Fig. 4 Bias maps of SWH (left panels) and SI maps of SWH (right panels) in comparison with HY-2A during the period starting from 2014 until 2018. **a** and **b** stand for ERA5 while **c** and **d** indicate WAVERYS

In deep ocean, the SI of SWH indicates remarkable values which range between 6 and 10%. As seen previously in Fig. 2, the WAVERYS shows smaller SI of SWH in comparison with the ERA5. This is particularly noticeable in Fig. 3 for the western boundary currents, the Agulhas current, and the periphery of the Indian basin, as well as for the equatorial Pacific current. This is mostly induced by accounting large-scale currents (see Section 4.1).

By splitting the SI scores by latitudes (not shown), we can easily see that the pole regions beyond 70° record values of SI of SWH between 12 and 14%. The pole areas are also subject to increase of errors for the retrieval of SWH from the HY-2A. The presence of more coastlines for the northern hemisphere degrades the SI values compared to the southern hemisphere (about 10% for northern mid-latitudes vs. about 7% for southern mid-latitudes). Similarly, the presence of coastlines plays an important role in the latitude-integrated results, with SI values between 10 and 15% for the longitudinal bands (− 90° E, − 60° E) (American continent), (0° E, 60° E) (Europe and Africa), and (100° E, 150° E) (Indonesia and Australia), whereas SI remains roughly around 8% elsewhere, notably around 7% in the Pacific because of the wide extent of the basin.

Figure 5 shows the performance of the ERA5 and WAVERYS in terms of HH index of SWH for several ocean areas of significant interest. The Indonesian region indicates the higher HH index of SWH with 22.5% of the WAVERYS whereas the ERA5 scores 17.7% for this region. As previously illustrated, this region forms a complex ensemble of small seas and archipelagos subjected to complex oceanic flow and tides, the latter not being taken into account carefully in both modelling systems. It can be mentioned that WAVERYS scores are also always better than those of the ERA5, regardless of the ocean region. Apart from wave physics and resolution, the absence of Jason-3 and Sentinel altimetry data in the ERA5 may handicap its results for the most recent years compared to the WAVERYS (see Fig. 14). This underlines the need for reanalyses to integrate as much reliable data as possible as soon as they become available. However, when we consider only the year 2014 where both the ERA5 and WAVERYS are using the same data, the comparison with the HY-2A indicates that the WAVERYS has globally a better SI of 8.6% with respect to 9.8% for ERA5. The improvement is also clearly

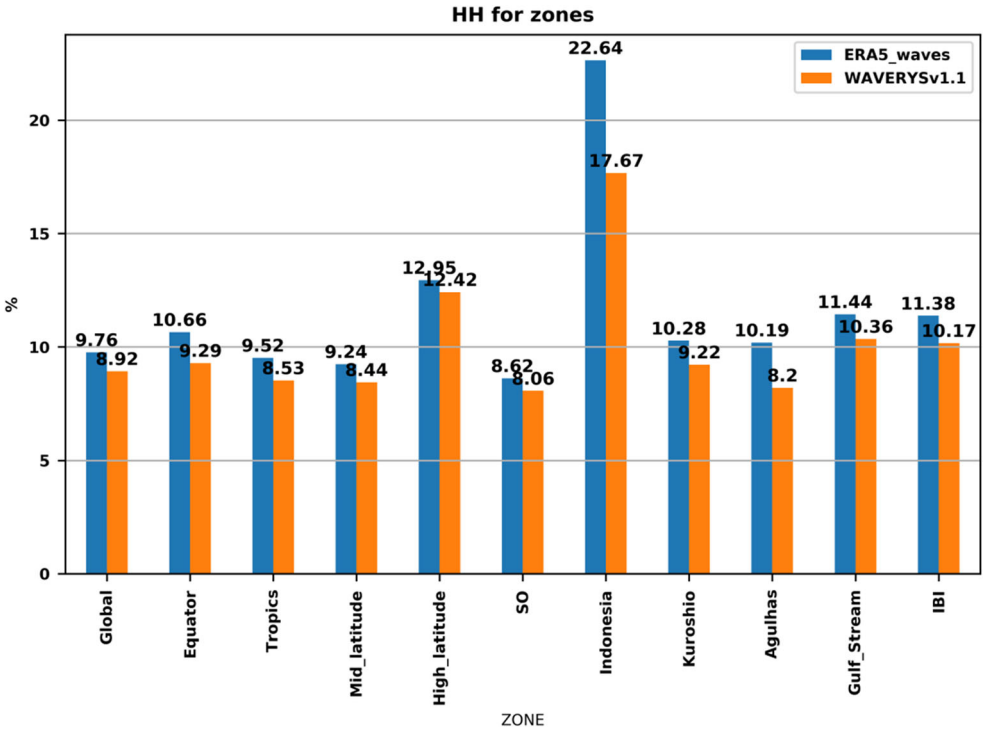

Fig. 5 HH index of SWH depending on specific ocean regions. ¼° ocean area masks are applied which can remove some coastal data. Similarly, latitudes outside (70° S, 80° N) are excluded. Ocean regions are defined according to the following split in latitudes: equator: |lat| < 3°; tropics: |lat| < 23.5°; mid_latitudes: 23.5° < lat < 66.5°; high_latitudes: |lat| > 60°. SO, all the Southern Ocean; Ibi, The Iberian and Biscay CMEMS zone

brought to light in Fig. 5 for ocean regions affected by currents. These results demonstrate that the WAVERYS is one of the best databases for the description of past sea states currently available for users.

4.1 Coastal validation

4.1.1 CMEMS buoys

The coastal validation was performed thanks to a set of wave buoys obtained from the CMEMS in situ Thematic Assembly Centre (TAC) product (Alfonso et al. 2019). This product includes wave observations aggregated and validated from the Regional EuroGOOS consortium (Arctic-ROOS, BOOS, NOOS, IBI-ROOS, MONGOOS) and Black Sea GOOS, as well as from National Oceanographic Data Centres (NODCs), Global Ocean Observing Systems (GOOS: Argo, GOSUD, OceanSITES, GTSPP, DBCP), and the Global Telecommunication System (GTS) used by the Met Offices. Figure 6 provides information on the spatial distribution of the data, as well as the available measurement time over the period 1993–2019. The buoys are mostly located near the coasts. The longest data series, more than 5 years, cover the east coast of Australia, Western Europe, and the west and east coasts of the USA. On the other hand, only short-period measurements, less than 6 months are available in South America, India, and the Mediterranean Sea around Italian coasts.

4.1.2 Method

Only buoys data that have passed all quality control procedure in real time are used in the following (quality control code equals to 1, see the related CMEMS product's QUality Information Document-QUID). Co-location between observation points and model points is achieved by spatially interpolating the model at the observation points and then temporally interpolating the observations on the model temporal axis to perform the comparison each of 3-h time step

4.2 Results

Figure 7 top panel shows a map that exhibits SI obtained for SWH and mean wave period (MWP) computed from the second moment at the in situ platform locations. MWP calculation is sensitive to a high-frequency cut-off which is around 0.4–0.5 Hz for buoys. In the WAVERYS, MWP calculation uses the entire spectral range of the model and this could lead to some discrepancies with buoys.

The average SI for the WAVERYS computed from the wave buoys is 20.7% for SWH and 14.8% for MWP. The results on SI can vary from one region to another, depending on specific local wave regime that dominates the area. For example, the North West American and Hawaiian coasts have respectively SI scores of 15.8% and 12.8% for SWH and 13.1% and 12% for MWP. This points out a good accuracy for long swell-dominated ocean regions. More precisely, when we consider the Hawaiian NDBC buoy 215 NM

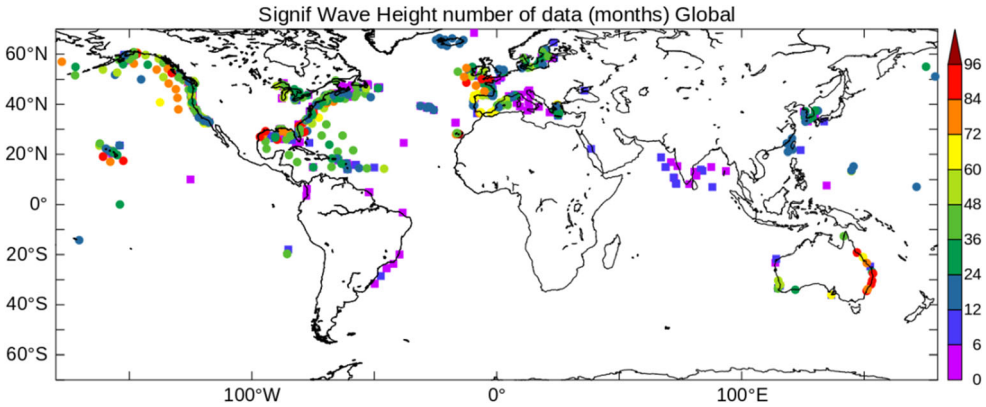

Fig. 6 Spatial distribution of CMEMS wave buoys for SWH and duration of measurements in months. Time series less than a seasonal cycle (1 year) are marked by a square instead of a circle

south-southwest from Hilo (51002), the SI of the peak period for waves larger than 150 m of wavelength is remarkably small, 9.4% for the year 2017. This result is typically achieved through SAR directional wave spectrum assimilation. Some buoy clusters on the other hand give larger SI values for SWH, more than 30%, likely because very coastal location such as in the Gulf of Alaska, in the Azores, in the Cap Verde Islands, and in the North Sea and some other locations off Italy coasts. From a global perspective, the best SI scores are obtained in tropical latitudes with 14.5% for SWH and 11.5% for MWP, where swells play again an important role in presence of weak winds.

The bottom panels of Fig. 7 are Taylor diagrams for SWH and MWP where the buoys are grouped by regions. In order to study coastal situations only, only the buoys where the local depth is less than 200 m have been selected.

For SWH, three groups of buoys can be identified. The first group are the ones already identified with the less skilled performance (the ones in Azores, North Sea, and Gulf of Alaska). This group performs with a correlation of 0.8 for normalized standard deviations of the order of 20%. It can be seen that the WAVERYS buoy equivalents in the Azores have too much variability with respect to the data, while the ones in the North Sea do not have enough. The second group of buoys has a correlation about 0.9 for standard deviations of the order of 10%, and encompasses tropical regions as well as Mediterranean and Baltic seas. The third group collects the remaining measurement points that perform best with correlation of 0.98 for a variance ranging between 5 and 10%. One can note that the variance for the better group is lower than the one of the data. The lesser performance for the first group of buoys is more likely related to imprecise bathymetry data and shelter effect that complicated coast lines induce. Further efforts at this level will be considered in future versions of WAVERYS with improved bathymetry.

For MWP, only the North Sea records a correlation of 0.7. The other measurement points have correlations between 0.8 and 0.9 for variances of the same order of the data, except in tropical areas where the variance is underestimated by about 15%.

Few buoys record mean wave direction (MWD), and Fig. 8 shows the results obtained by the WAVERYS in terms of mean differences, RMSD, and correlation coefficient with observations. MWD represents the average direction where most of the wave energy propagates. Deviations from observations can therefore give an indication of poor directional spread, and sometimes errors induced by multi-modal wave systems. Concerning mean differences, following the convention of CMEMS wave files (0° = North, 90° = East), a positive (resp. negative) difference means waves arriving too far from the right (resp. left). The biases of wave direction are on average small of roughly 5°, and the strongest biases concern the Azores and the Canarias Islands, with more than 20° of deviation. It can be noted that the western North Atlantic and the Gulf of Mexico have positive directional biases, while they are negative biased further south in the Caribbean Sea (amplitude range < to 10°). The biases of MWD for the European coasts alternate between positive and negative, which underlines the variability of the wave systems encountered in this ocean area.

With regard to RMSD of MWD, the ocean areas with satisfactory results less than 30° are located in the Bay of Biscay, off shore of Ireland, and in the Caribbean. The less precise areas in terms of variability are again the Cape Verde and Azores islands, with RMSD around 80°.

For the correlation coefficient of MWD, high and mid-latitudes indicate a better values (greater than 0.6) compared to the tropics (smaller than 0.5). This is surprisingly the opposite of what we have found for SWH. It is probably related to the presence of stronger winds in higher latitudes, which induce better capturing of direction for dominant wind-sea wave systems. Note that the MWD has been treated as a scalar for correlation, which can lead to errors when wave trains oscillate around the north. In other respects, very small correlations (> to 0.2) are found in the tropical Atlantic, French Polynesia, Hawaii, and off CA, USA.

Table 1 compares the statistical scores obtained between the WAVERYS and ERA5 for SWH whenever the

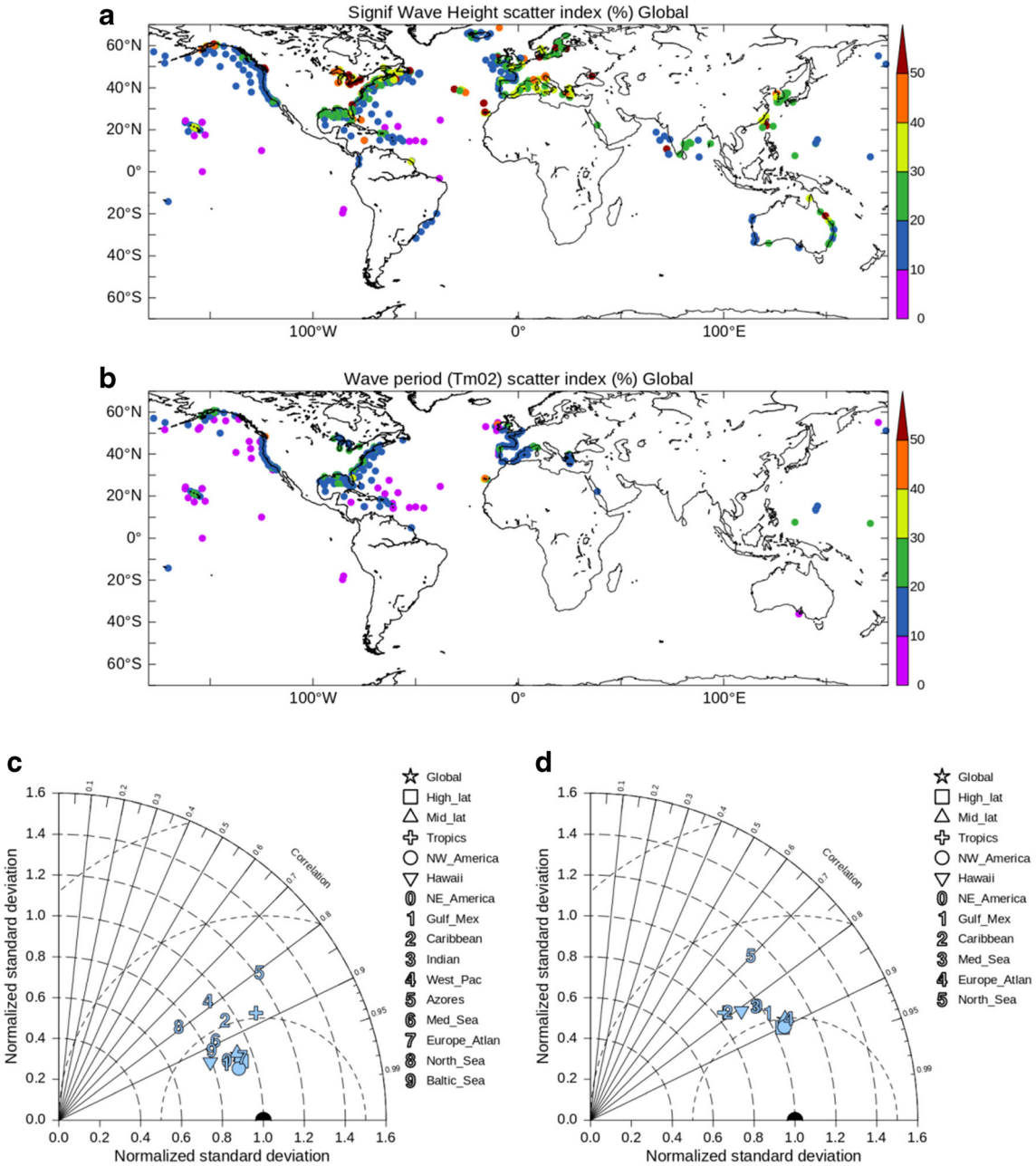

Fig. 7 Top panel: mean SI scores obtained by WAVERYS for each CMEMS wave buoy, for SWH (**a**) and MWP (**b**). Bottom panel: Taylor diagram obtained by classifying results by region or basin. Results obtained for SWH (**c**) and MWP (**d**). Only coastal buoys, i.e. buoys positioned on a layer of water less than 200 m deep, are used in Taylor diagrams

comparison is feasible for the 1993–2018 period. It shows that the WAVERYS is always better than the ERA5 compared to buoys, regardless of the coastal situation, region, or latitude. It can be noted that the wind measurements from most of in situ buoys were assimilated in ERA5, which suggests a reliable wind sea for both systems near the buoys.

We have also examined the comparison with the buoys through wave rose diagrams. These diagrams are useful tools to visualize the dominant wave regimes, and whether the wave model is able to reproduce them or not. We show as illustration two cases were the model performs satisfactorily as illustrated in Fig. 9.

The first example is a mooring off shore of north-western tip of California. The regular wave regime measured by the buoy is a swell propagating towards the south-east and spreading over about 90° on each side. Sixty-percent of the occurrences occur in a 30° cone centred in the south-east direction. Focusing on these wave systems, the overall height distribution is about 50% of waves between 2 and 5 m, 35% of waves between 1 and 2 m, and 10% of waves between 0.5–1 m.

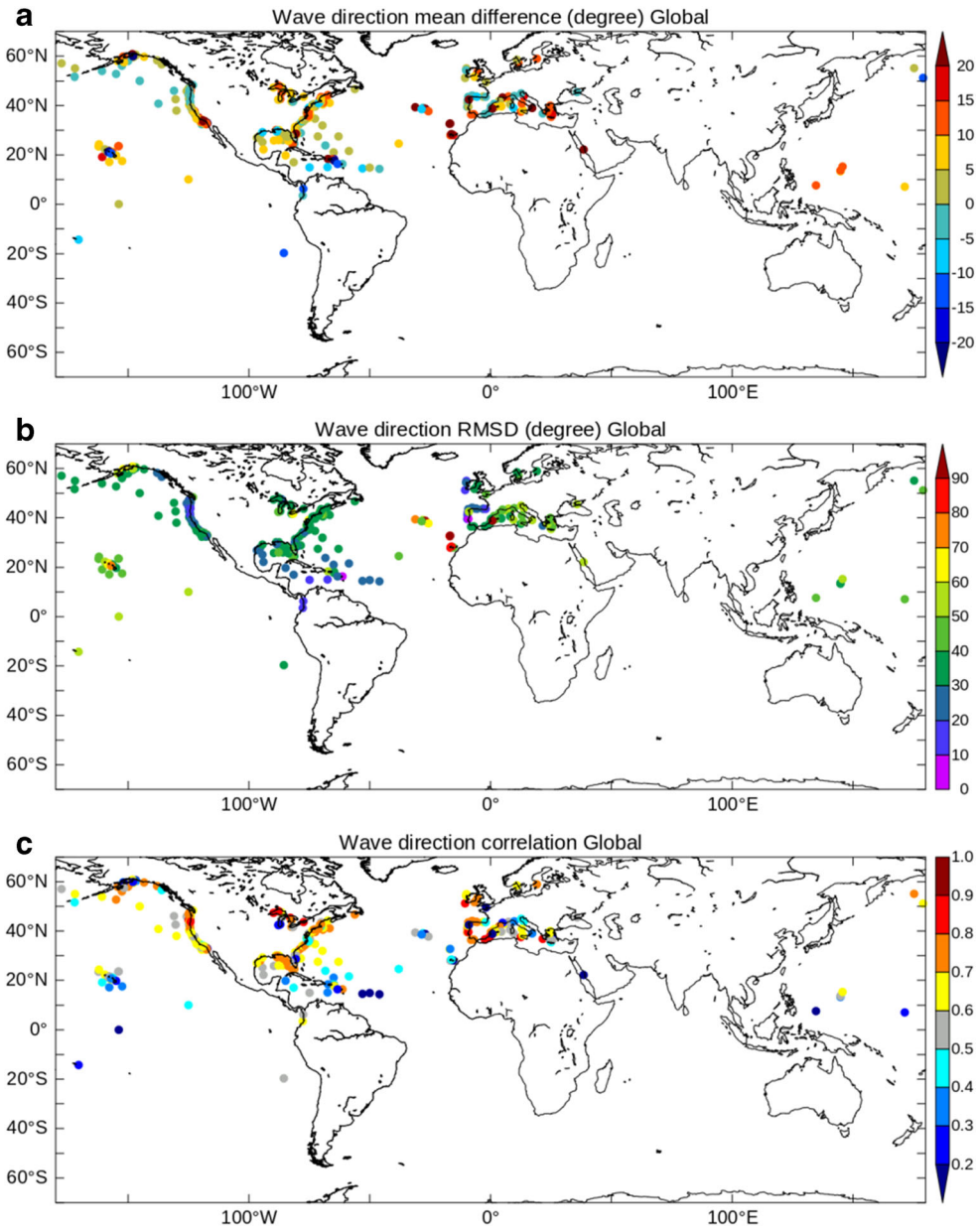

Fig. 8 Mean differences (**a**), RMSD (**b**), and correlation (**c**) for MWD between WAVERYS and CMEMS buoys at each measurement point. MWD was treated as a scalar for correlation, but RMSD take into account circularity

Waves between 5 and 10 m represent only a small fraction of the occurrences. The WAVERYS reproduces relatively well the observed wave regimes, although the model is more constrained towards the south to south-east directions (25% of the occurrences, against 20% for the buoy), with less directional spreading. Waves propagating eastward disappear completely in the WAVERYS for instance. Finally, the WAVERYS seems to produce more waves in the 1–2-m range than what is measured by the buoy.

The second example comes from a buoy situated in the Baltic Sea, at Huvudskar (Sweden). The wave rose scored by the buoy consists of a dominant west to south-west regime with a directional spread of 30° which represent 45% of the total recorded occurrences. A second wave regime propagates north-eastward for about 35% of the total occurrences. The other propagation directions are less frequent, and one can mention the presence of waves smaller than 20 cm propagating towards directions between the west-northwest to the east-northeast, more likely due to local wind sea system. The wave rose obtained with the WAVERYS gives again fewer occurrences in the dominant wave direction observed by the buoy. A more scattered sea state is obtained by the reanalysis, with an increase of occurrences in non-dominant directions (from the buoy record point of view) by a few percent. Small waves below 20 cm are also more present in the WAVERYS, probably induced by uncertainties related to local wind forcing.

Table 1 Comparison of equivalent statistics for SWH obtained by WAVERYS and ERA5 using in situ buoys. Only the strictly concordant points between the two reanalyses over the 1993–2018 period were used

Zone	Statistics	WAVERYS	ERA5 wave
Global	Bias (cm)	−0.046	−0.055
	SI (%)	19.588	21.279
	Correlation	0.959	0.953
Shelf	Bias	−0.024	−0.019
	SI	24.782	26.768
	Corr.	0.941	0.931
Open Sea	Bias	−0.066	−0.088
	SI	16.167	17.672
	Corr.	0.968	0.964
High Latitudes	Bias	−0.064	−0.102
	SI	18.512	19.894
	Corr.	0.965	0.962
Mid-latitudes	Bias	−0.043	−0.046
	SI	20.507	22.306
	Corr.	0.956	0.949
Tropics	Bias	−0.033	−0.036
	SI	13.922	15.658
	Corr.	0.938	0.922

Most of the measurement points have demonstrated the good performance of the WAVERYS in reproducing local wave regimes with wave roses.

5 Features of WAVERYS

5.1 Impact of ocean currents

An interesting feature of the WAVERYS is the forcing by ocean currents. Four years (2014–2017) of a twin experiment without including oceanic currents (WAVERYS_NOCUR) has been produced to study their impact on the system performance and thus identify the areas concerned by wave-current interactions. Figure 10 shows a percentage gain map obtained on the SWH HH index between the WAVERYS and this WAVERYS_NOCUR simulation. The gain is measured with the similar validation procedure than in Section 2.1, with the HY2-A altimeter as supporting data. The improvement in large current structures such as equatorial currents, western boundary currents, and ACC are clearly visible with a gain of around 20 to 40% in these areas.

In terms of SWH, SI values, including oceanic currents, lead to an average improvement for SWH by 3.2% for the global ocean, by 4.7% for the Equatorial band, and by 11.6% for the Agulhas Current area. This demonstrates the relevance of accounting ocean currents at global scale in order to better forecast the sea state, as already advocated by (Bidlot 2010, 2012b). Despite an overall improvement, ocean regions directly concerned by strong currents are the most improved ones, notably when currents are flowing along with, or opposite to swell regimes, such as the Agulhas Current, the North Brazilian Current, and the East Pacific and Atlantic Equatorial currents. SI improvement can even reach 25% locally in those situations. Benefits from western boundary currents like the Gulf Stream; the Kuroshio; and, their southern counterpart, the Antarctic Circum polar Current (ACC) are clearly highlighted with SI improvements always greater than 15%. The Indian Ocean appears to be a special place for wave-current interactions in comparison with other ocean basins, probably because of its northern land border, which channels typical coastal flows that southern swells encounter on their way to the coast, as in the Mozambique Channel, the Bay of Bengal, and the West Timor Sea. There is no visible degradation caused by currents on the SI and HH of the SWH (negative values in Fig. 10 are identified as noise in areas depopulated by currents). We can nevertheless add that the normalized RMSE improvement map (not shown), which contains some of the biases, shows degradations of a few percent in the following areas: Arabian Sea, east of the Philippine, eastern Timor Sea, and to lesser extent in upwelling zones such as Peru-Chile and Gulf of Guinea. These zones have been identified in Mercator systems as biased zones for currents by comparison to surface drifters (Marie Drevillon, personal communication).

But one can ask what the impact of ocean currents on wave parameters is? The left panels of Fig. 11 shows the average differences obtained in terms of SWH, WMP, and MWD between the WAVERYS and WAVERYS_NOCUR simulations. The differences for each wave parameter show nearly similar structures that reflect the global ocean circulation. In the path of noteworthy currents, the refraction of wave trains introduces typical "positive/negative" differences on each side of oceanic flows, related to current-induced horizontal gradients. The differences are of the order of a few centimetres for SWH, a few tenths of seconds for WMP, and a few degrees for WMD. As seen previously, the Indian Ocean is the most affected by wave-current interactions, where the differences reach a maximum of 15 cm for SWH, 1.2 s for MWP, and 15° for MWD, respectively, for the most concerned places. Similar ranges are also seen for the North Brazilian Current. For the open ocean, the use of surface currents is accompanied by a slight global strengthening of SWH and periods. For directions of wave origin, the upper branches of the western ocean circulation (Gulf Stream, Kuroshio, ACC) seems to fold the wave trains towards the equator, while the lower branches of the subtropical gyres cause poleward deviations.

Swells are an interesting case study for current-wave interactions because their stability allows them to propagate over

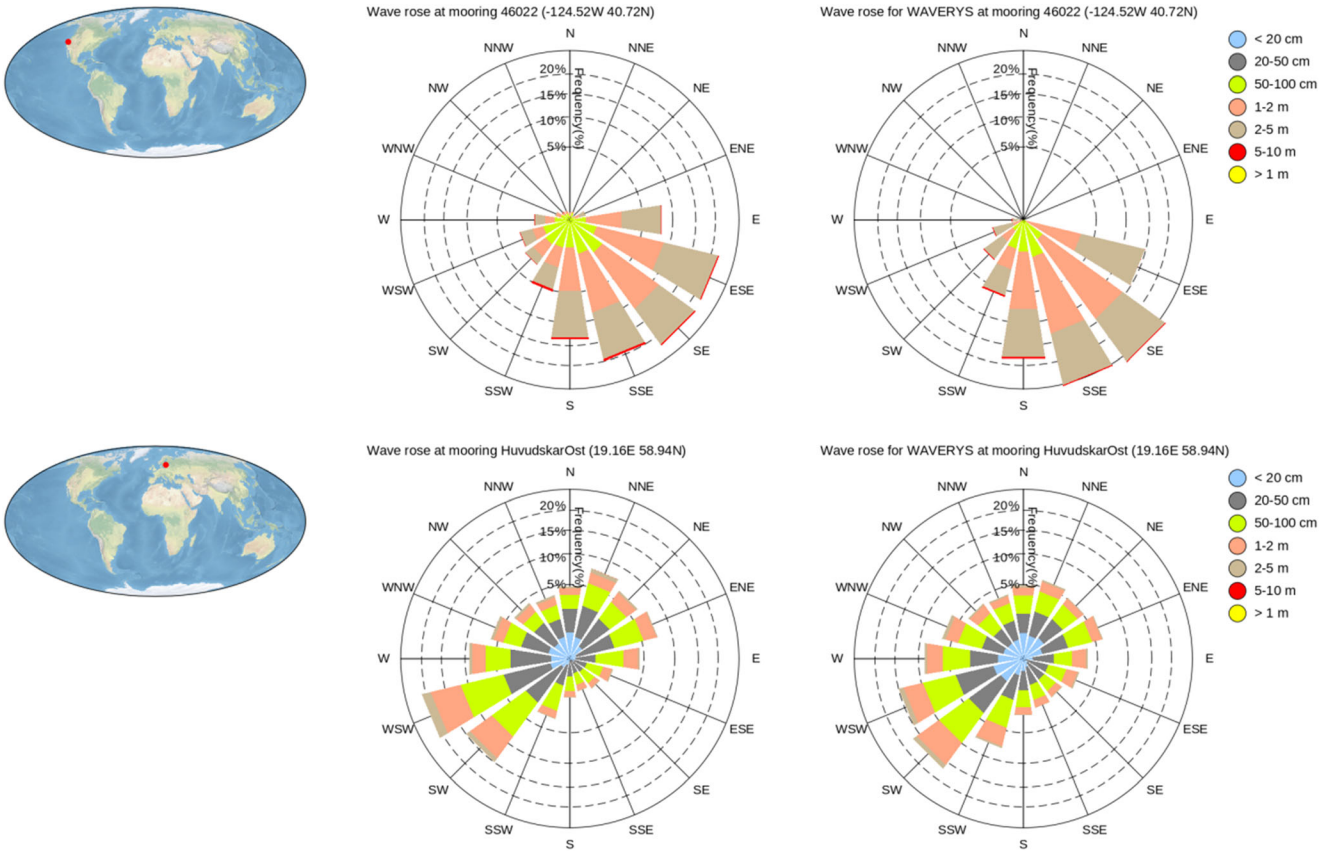

Fig. 9 Wave roses computed from CMEMS wave buoys (left) and WAVERYS (right). The radial scale gives the frequencies of occurrence of wave height/direction (note that the scale is not linear). Directions are given in the oceanographic convention (i.e. direction of propagation). A red point shows the buoy location on the left maps. Top: mooring no. 46022 in California ocean region, bottom: HuvudsarkOst mooring in the Baltic Sea

thousands of kilometres for time period of roughly 10 days, and thus to encounter several current systems. Nevertheless, the longer the wavelength, the less sensitive the wave trains to currents are. The right panels of Fig. 11 examine the occurrences of differences for the primary swell partition between the WAVERYS and WAVERYS_NOCURR. The occurring criteria for the differences are the following: greater than 10 cm for SWH (b), greater than 1 s for the MWP (d), and

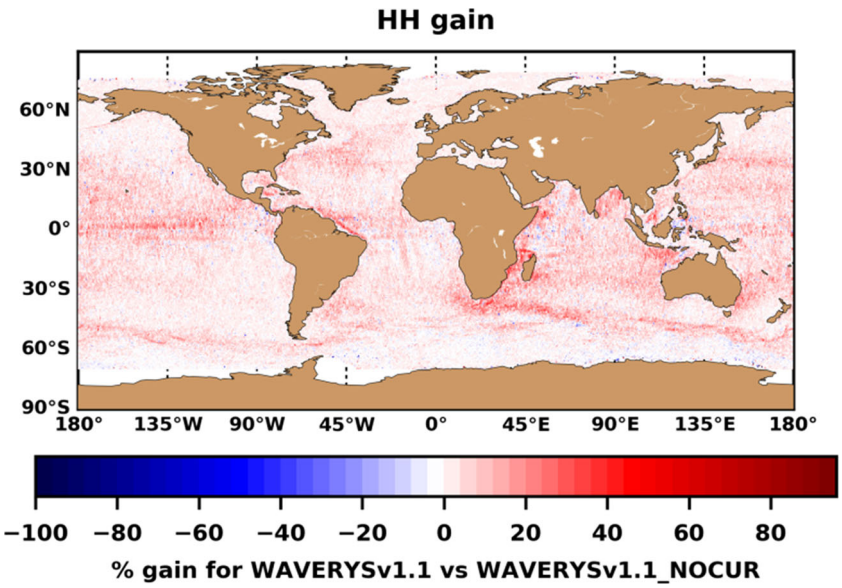

Fig. 10 HH index percentage gain map for SWH between a 4-year WAVERYS period (2004–2017) compared to an identical run without oceanic currents

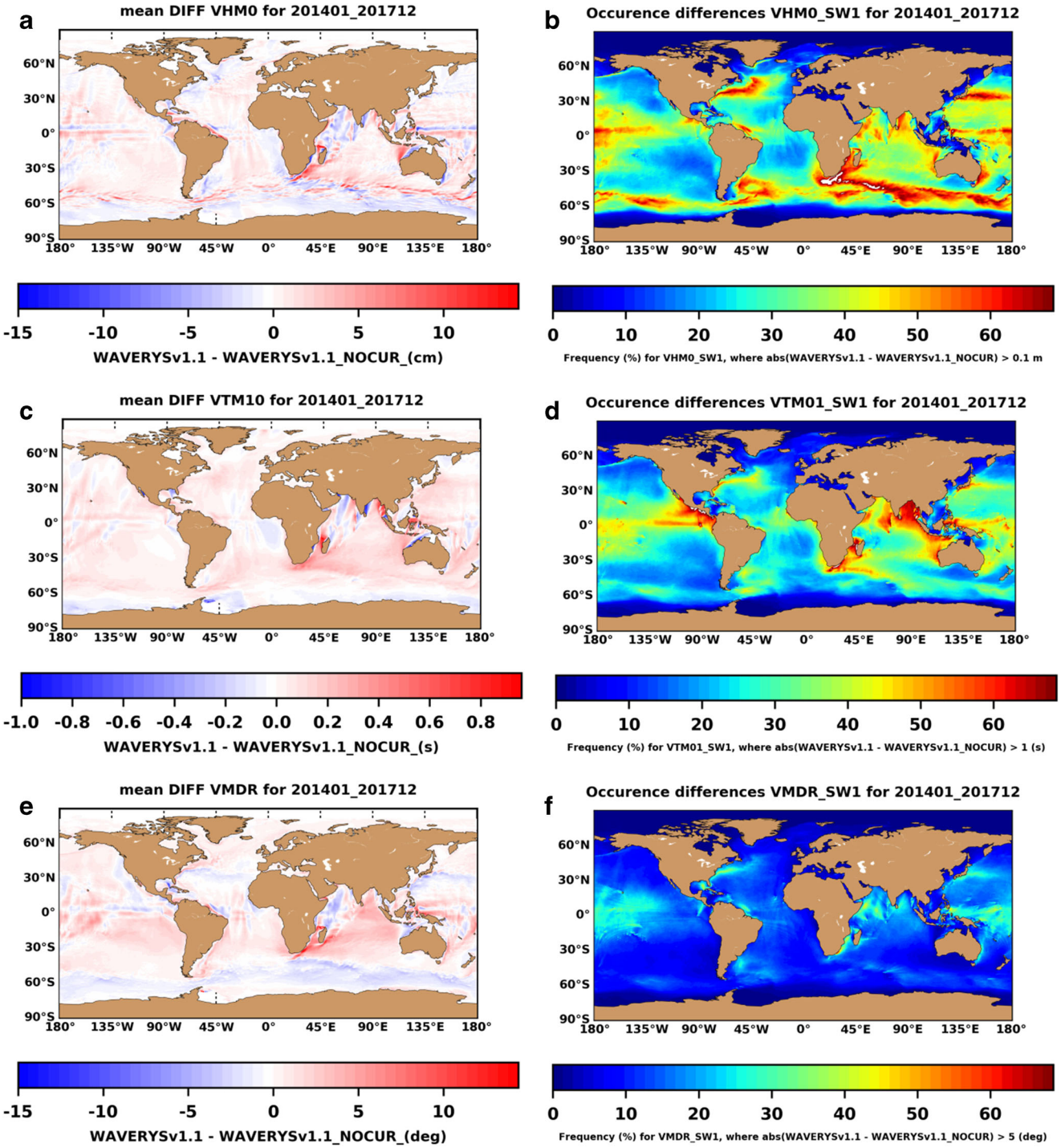

Fig. 11 On the left panels: average differences between WAVERYS and a similar run without currents for **a** significant wave height (SWH), **c** mean wave period (MWP), **e** mean wave direction (MWD). WAVERYS_NOCUR is taken as a reference, so that the positive values for SWH or period (resp. direction) correspond to an increase (resp. deviation to the right) of WAVERYS with respect to it. On the right panel: probability of occurrence (in %) where the differences for the primary swell between WAVERYS and WAVERYS_NOCUR exceed a certain threshold: **b** 0.1 m for SWH, **d** 0.5 s for MWP, **f** 15° for MWD

greater than 5° for the MWD (f). Results show that wave-current interactions meet these criteria for about 60% of occurrences in large-scale currents. Eastern shore currents, inland seas, and the open ocean (apart from equatorial currents) produce weaker occurrences of the order of 10–20%. Occurrences of period differences greater than 1 s are rather localized at the equator and related to the crossing of the equatorial belt by subpolar swells. For difference in swell periods,

the Indian Ocean is again very marked in terms of occurrences due to the refraction of the southern ocean swells by complex coastal circulations in the northern part of the basin. For swell directions, a difference of more than 5° has an occurrence of 30% in the very vicinity of the currents. Interestingly, it is possible to spot in Fig. 11f refraction artefacts caused by the bending of swells by equatorial currents.

As waves evolve on oceanic flows, both width and vorticity of the encountered oceanic structures condition the resulting deflection angle (Gallet and Young 2014). It should be noted that the WAVERYS' resolution allows it to integrate equatorial eddies, but eddies smaller than 50 km shall not be well-introduced, notably for higher latitudes where the local Rossby radius shrinks. It must be kept in mind that apart from the equator, the effect of refraction by the mesoscale activity is underestimated in WAVERYS.

5.2 Climatology, trends, and extreme events

It is admitted that a minimum period of 20 years is necessary to investigate wave extremes (Mazas and Hamm 2011). With more than 25 years of wave products, the WAVERYS can be helpful to analyse past wave climate and to diagnose mechanisms that drive changes in wave climate projections.

Figure 12 shows the climate characteristics of the WAVERYS for SWH and WMP, namely the climate mean, the 90th percentile, and the trend of the total time series. On these maps, the poles have been deliberately omitted due to poorly represented ocean-wave-ice interactions.

Concerning the climate mean, the typical global distribution of waves is found, with the highest waves (greater than 4 m) situated in the westerly wind track, the lower waves (2 m) in the trade wind system, and the weaker ones encountered in semi-enclosed seas or in equatorial belt. The longest waves, with average period of 14 s, are representative of the most important distances travelled by polar origin swell. They are found in the eastern side of subtropical basins, more likely in the south Pacific and Indian oceans due to reinforce winds and extended fetch. Fetch also conditions periods elsewhere, with variation from 6 to 8 s for closed seas to sub-basin scale propagation.

The 90th percentile (the maximum value for 90% of occurrences) is a good proxy for the maximal values that can realistically occur for waves. Patterns are nearly identical to the average distribution of SWH, with values of 7 to 8 m for subpolar depressions, and waves of about 2 to 3 m at the equator. In terms of MWP, we can see easily that fetch-limited areas and enclosed seas are more affected by shorter waves with range between 6 and 8 s. For the longest wave maximums they are slightly increased from 14 to 15 s in comparison with the climate averages for the longest waves. In other respects, waves of range between 10 and 12 s are likely to occur in most of the open ocean.

With regard to SWH, trends over the whole time series are of the order of ± 1 cm per year, which is relatively small compared to the typical range of sea waves (order of 1 m). Positive SWH trends are found mostly in the tropical belt, as well as in the Atlantic Ocean, North Indian, and Western Pacific, which indicates presumably strengthening of the trade winds and cyclonic activity. The trend map of SWH for the ERA5 over the same years (visible in Appendix Fig. 17) shows identical patterns to that of the WAVERYS. The notable difference being that the trends in North Indian are rather negative for the ERA5, which suggests differences in wave train patterns related to monsoon or cyclones. Timmermans et al. (2020) recently showed trend of SWH obtained from running with the ERA5 forcing a wave hindcast (no data assimilation) with the stand-alone version of the ECMWF wave model (ECWAM) equipped with ST4-like physics close to the WAVERYS. Those authors attributed the negative SWH trends in the Central Pacific to changes in extra-tropical storm tracks. Aarnes et al. (2015) also showed that the ERA-Interim had erroneous trend due to assimilation of irregular altimeter data; both the ERA5 and WAVERYS may show similar, smaller effects, but this is beyond the scope of this study.

Trend patterns for MWP are strongly correlated to the ones for SWH. It can be seen for instance the increase of the average wave periods by a few tens of milliseconds per year in the Atlantic, Indian, and West Pacific oceans. Figure 12 f also reveals a more pronounced negative trend for wave period at the equator, on the eastern edges of the basins, particularly in the Pacific Ocean. These locations are identified as seas where the longest swells occurred. More investigations are needed to understand the causes of such trend. MWP's trends for the ERA5 (Fig. 17) are similar to those of the WAVERYS, except that the lengthening of periods are less pronounced in North India and Indonesia.

In other respects, it may be interesting for users to know how the WAVERYS behaves in extreme event conditions such as cyclones, as they are also suggested to impact the trends in Tropics. Cyclone modelling has always been a challenging task because of the sensitivity of the coupling processes between the ocean, waves, and the atmosphere. For instance, the main driving force of cyclones comes from evaporation and heat fluxes which are mainly limited by the sea surface roughness, and thus the waves. But intense spiral winds generated by cyclones spatially modify the fetch and create a complex sea composed simultaneously of energetic wind-sea and swell (Li et al. 2012; Young 2017). We were interested in looking at cyclonic events from 2012 to 2018 on the basis of the IBtracks data (Knapp et al. 2010).

The top panel of Fig. 13 illustrates the SWH map of the WAVERYS during cyclone Claudia (Indian Ocean) on December 10, 2012, at 0:00 UTC. At this date, the event is at its peak with wind speed greater than 50 m/s, and SWH from the WAVERYS of about 8 m near the cyclone eye. The

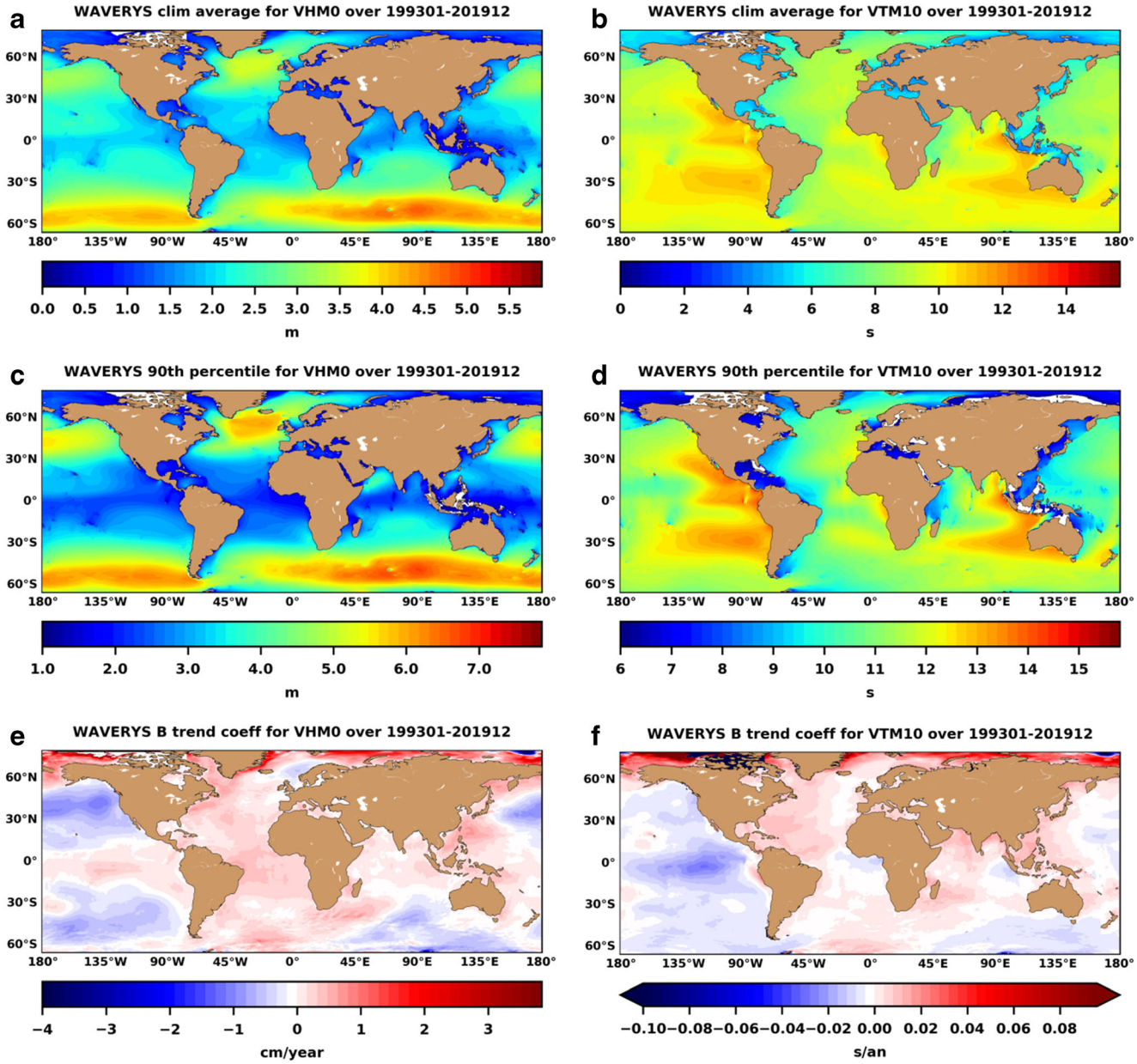

Fig. 12 Climate statistics for SWH (left panel) and MWP (right panel) time series. Panels consist of climate mean (**a**, **b**), 90th percentile (**c**, **d**), and trends (**e**, **f**)

range of modelled SWH is between 4 and 6 m within a radius of 5° from the cyclone eye.

The middle panel of Fig. 13 shows the difference of SWH modelled by the WAVERYS and ERA5 for the same date. It can be easily seen that the impact of the cyclone Claudia is enhanced in the WAVERYS with respect to the ERA5, with a difference of SWH ranging between 30 and 60 cm near the cyclone eye. In fact, for all the cyclonic events that we have looked at, SWH from the WAVERYS is always larger than the one provided by the ERA5, except in a crown located in the immediate vicinity of the eye. This is also illustrated by the bottom panel of Fig. 13.

This panel indicates the PDF of SWH for the WAVERYS and ERA5 computed from a 5°×5° sliding sub-domain centred on the trajectory of each cyclone over 2012–2018. This represents more than 515 events for 4113 days of data. Due to the size of the 5°×5° sub-domain, only a quite local response to the cyclone is expected, so that long cyclonic swells are not considered. From the two PDF curves, we can see that on one the hand, the WAVERYS produces fewer SWH cases in the range of 1–2.5 m than the ERA5. On the other hand, the WAVERYS gives more cases than the ERA5 for larger SWH between 2.5 and 8 m, which is more related to cyclonic wave range.

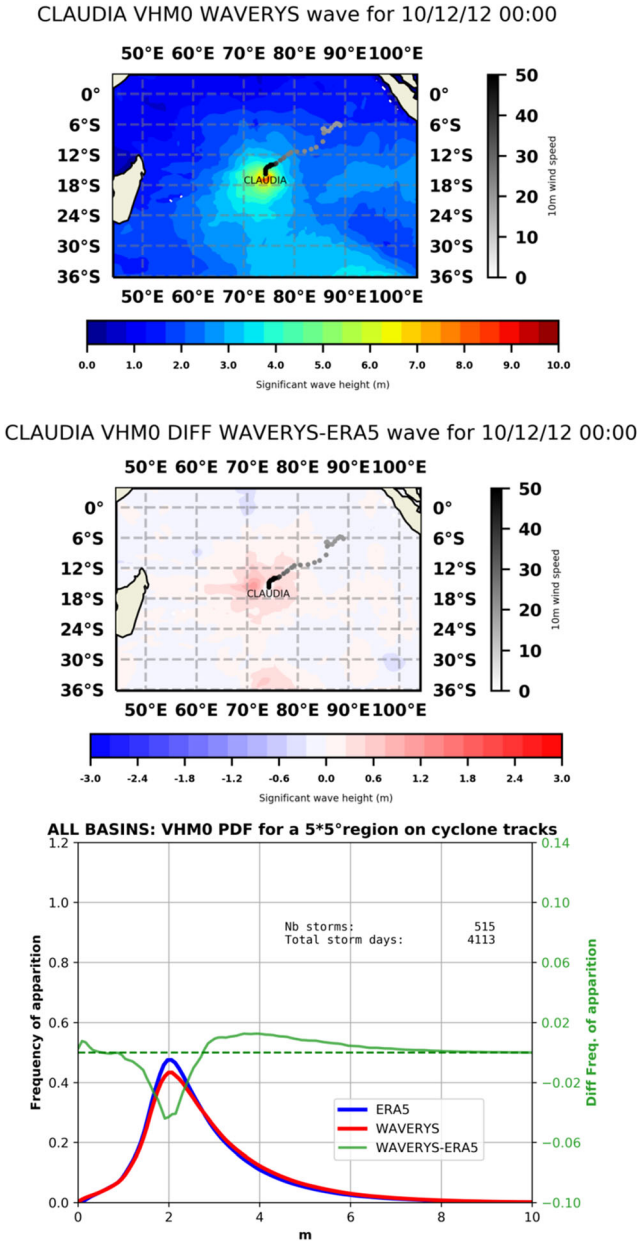

Fig. 13 Top: SWH map during hurricane Claudia for WAVERYS. The trajectory of the cyclone is overlapped with colour scale corresponding to the wind speed at 10 m. Middle: difference of SWH between WAVERYS and ERA5. Bottom: PDF of SWH for WAVERYS, ERA5, and their difference (in green) on a 5° sliding box around the trajectory of all the cyclones available for the IBtracks database for 2012–2018

This section on cyclones is intended to be illustrative and calls for a more in-depth study to qualify the two reanalyses with respect to extreme events. We believe that the WAVERYS can be an interesting source to study cyclones on multi-year scales, but the temporal resolution of the atmospheric forcing and the coupling with ocean thermodynamics remain crucial points to be addressed in future versions to better capture these phenomena.

6 Discussion and conclusion

This paper presents the WAVERYS, the first global wave reanalysis of the CMEMS. The products describe past sea states from 1993 to 2019 with a spatial resolution of 1/5° and 3-h mean wave parameters and wind-sea/swell partitioning parameters. The quality of the WAVERYS has been assessed by (i) comparing the analyzed SWH with SWH from the altimeter HY-2A as independent data in open ocean during the period of 2014–2018; (ii) comparing the mean wave parameters with CMEMS in situ buoy measurements (coastal data validation during the period of 1994–2019).

For the open sea, the WAVERYS performs globally with a scatter index of 8.8% with relatively low biases of about 3 cm. This represents 8.3% of improvement in comparison with the ERA5 wave reanalysis.

Because of the limitation of the 1/5° spatial resolution and the complexity of the ocean-wave interactions near the coasts (e.g. instability of currents, and tides), the system performs less well in shallow waters and in semi-enclosed sea, where the scatter index of SWH can reach 18%. Nevertheless, the validation has shown the good contribution of oceanic currents for the sea state accuracy in current-dominated ocean areas such as the Agulhas Current, the North Brazilian Current, with local SI improvements up to 40%. More generally surface currents have a significant impact on the propagation of swell, whose rays are bent when encountering large current systems. It can nevertheless be pointed out that the resolution of application of the currents (1/5° although they have been modelled at 1/12°) limits the best use of typical local eddy scale outside the tropical zone. Similarly, interactions with the tide are another source of missing diffusion (Ardhuin et al. 2012) and could greatly contribute to improve the wave forecast on shelf.

Direct comparison with wave buoys revealed the good description of some typical local regimes for the WAVERYS. The good results from sites exposed to long swells, like the North West US coasts and Hawaii, can be particularly mentioned. However, the WAVERYS has difficulty in reproducing exactly the variability observed by the buoys in coastal areas. This limitation could be due to uncertainties in wind forcing variability. A potential room for improvement on this point would be to use wind gust forcing as suggested in recent works (Timmermans et al. (2020), J.R. Bidlot personal communication).

The wave climatology of the WAVERYS is in good agreement with what is described in the literature, and relatively close to the one from the ERA5 wave data. The use of the WAVERYS wave products can contribute to wave climate trends in several ocean regions. There is still a need of dedicated validation for extreme wave events such in cyclone conditions. Furthermore, the space-time resolution of wind forcing may not be good

enough to accurately reproduce extreme events in terms of intensity and variability.

The WAVERYS is planned to be updated (version 2) next year with several noticeable improvements, like a refinement in spatial and temporal resolution (1/10°, 32 directions), as well in bathymetry. Better assimilation scheme, combining directional wave spectra from different sensors such as the SAR of Sentinel-1 and SWIM of CFOSAT, will be implemented. We will also include directional wave spectra from the SAR of Envisat mission (2002–2012) in the assimilation system. The CMEMS foresees temporal extensions of reanalyses every 6 months. Useful information for users is already available on the QUID document of the WAVERYS, available on the CMEMS website.

Acknowledgements The authors would like to thank Isabel Garcia-Hermosa (Mercator-Ocean International) for her review of the QUID of the WAVERYS product, which was the first step to the writing of this article. CNES provided us with level 2 wave data of the HY-2A mission. We also thank the two anonymous reviewers and the editor whose comments and questions helped greatly to improve our presentation.

Appendix 1: ST4 physics settings

Table 2 settings for ST4 physics used in the wave model

SDSC2	−2.6 E-05
SDSC3	0.8
Tauwshelter	0.4
Tailfactor (FXFM3)	4
Betamax	1.48

Appendix 2: Assimilated altimetry data

Figure 14 shows for each altimetry mission the period of application for the WAVERYS. It can therefore be seen that the most constrained periods are between the years 2002–2006 (5 altimeters) and 2016–2018 (4 altimeters + SAR sentinel 1). Figure 15 shows an illustration of the spatial coverage of the assimilated altimeter data over the course of a day. Because of the orbits' offset and entanglement, the mesh can be more or less loose or tightened over an area within a day.

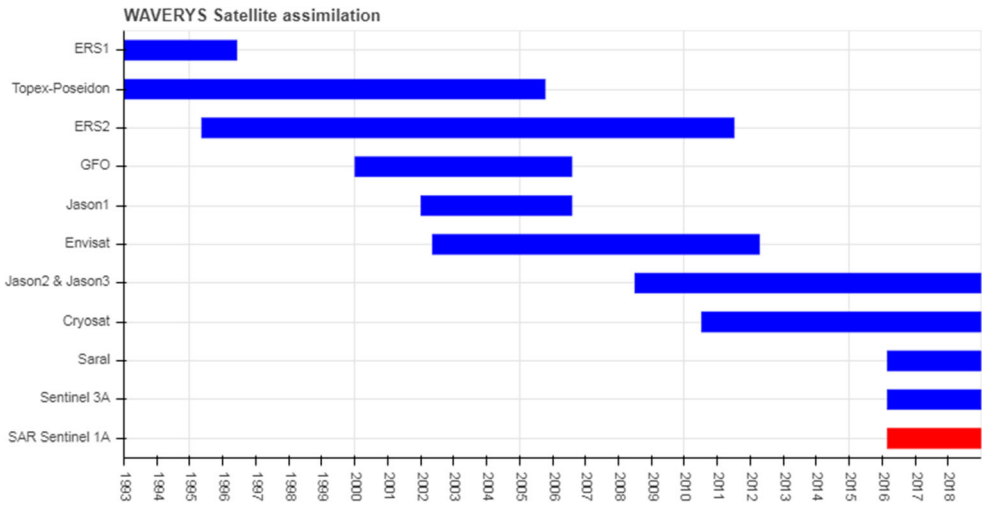

Fig. 14 List of assimilated satellite data and their period of use. Altimeters are in blue and SAR is in red

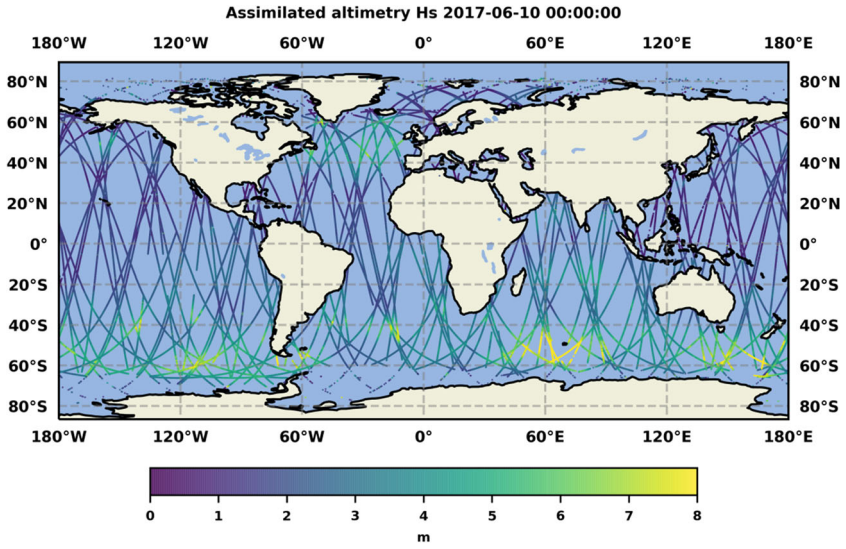

Fig. 15 Map of all the SWH altimetry tracks assimilated in the system for June 10, 2017

Appendix 3: Correction of HY-2A SWH

In this section, we implemented a comparison between the Jason-2 and HY-2A significant wave heights. The analysis is performed at crossovers of ground tracks of the two altimeter missions with a time window of 2 h. We computed super-observations in a box of grid size of 0.5° for the comparison between the Jason-2 and HY-2A. It has been collected 6192 data during the period January to June 2015. Figure 16 shows the scatter plot of SWH from the Jason-2 and HY-2A. It is easy to see that there is a strong underestimation of SWH of HY-2A in comparison with Jason-2. The bias increases for high waves. We then computed an orthogonal linear regression which gives the a and b coefficients of 0.944 and − 0.01, respectively. This relation is used in order to remove the bias of SWH for HY-2A.

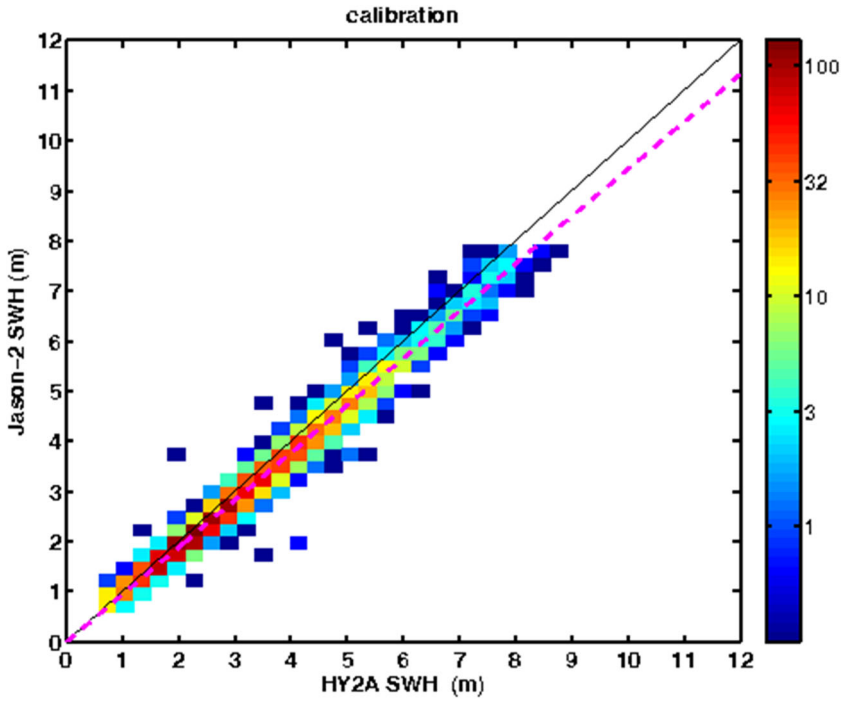

Fig. 16 Scatter plot of SWH from Jason-2 and HY-2A. The colourbar indicates the density of data, while the purple dashed line shows the orthogonal linear regression with $a = 0.944$ and $b = -0.01$

Appendix 4: ERA5 SWH and mean wave period trends

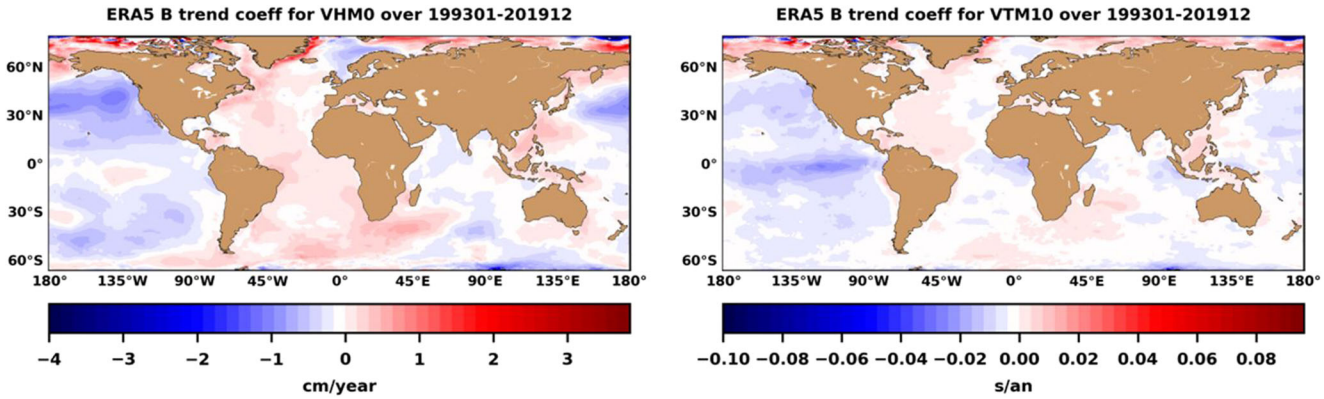

Fig. 17 Trends for SWH and MWP for ERA5, calculated over the same period and following the same method as in Section 3.2 (compared to Fig. 12e and f for WAVERYS)

References

Aarnes OJ, Abdalla S, Bidlot JR, Breivik Ø (2015) Marine wind and wave height trends at different ERA-interim forecast ranges. J Clim 28:819–837. https://doi.org/10.1175/JCLI-D-14-00470.1

Abdalla S, Janssen PAEM (2017) Monitoring waves and surface winds by satellite altimetry applications. In: Stammer D, Cazenave A (eds) Satellite altimetry over oceans and land surfaces, CRC Press. Taylor & Francis Group, USA, pp 379–424

Alfonso CM De, Manzano F, Gallardo A (2019) CMEMS quality information for reprocessed in situ product (WAVES) INSITU_GLO_WAV_REP_OBSERVATIONS_013_045. https://doi.org/10.13155/58696

Aouf L, Lefèvre JM, Hauser D (2006) Assimilation of directional wave spectra in the wave model WAM: an impact study from synthetic observations in preparation for the SWIMSAT Satellite mission. J Atmos Ocean Technol 23:448–463. https://doi.org/10.1175/JTECH1861.1

Aouf L, Hauser D, Tison C, Mouche A (2016) Perspectives for directional spectra assimilation: results from a study based on joint assimilation of CFOSAT synthetic wave spectra and observed SAR spectra from Sentinel-1A. In: International Geoscience and Remote Sensing Symposium (IGARSS), pp 5820–5822

Aouf L, Dalphinet A, Law-Chune S, Drillet Y (2018) The upgraded CMEMS global wave system: IMPROVEMENTS and efficiency for ocean/wave coupling. In: EGU General Assembly

Aouf L, Dalphinet A, Law-Chune S, Drillet Y (2019) Evaluation of surface currents forcing in CMEMS wave system. In: ESA Workshop of World ocean circulation-Users

Ardhuin F, Rogers E, Babanin AV, Filipot JF, Magne R, Roland A, van der Westhuysen A, Queffeulou P, Lefevre JM, Aouf L, Collard F (2010) Semiempirical dissipation source functions for ocean waves. Part I: definition, calibration, and validation. J Phys Oceanogr 40:1917–1941. https://doi.org/10.1175/2010JPO4324.1

Ardhuin F, Roland A, Dumas F, Bennis AC, Sentchev A, Forget P, Wolf J, Girard F, Osuna P, Benoit M (2012) Numerical wave modeling in conditions with strong currents: dissipation,refraction, and relative wind. J Phys Oceanogr 42:2101–2120. https://doi.org/10.1175/JPO-D-11-0220.1

Ardhuin F, Gille ST, Menemenlis D, Rocha CB, Rascle N, Chapron B, Gula J, Molemaker J (2017) Small-scale open ocean currents have large effects on wind wave heights. J Geophys Res Ocean 122:4500–4517. https://doi.org/10.1002/2016JC012413

Barbariol F, Bidlot JR, Cavaleri L, Sclavo M, Thomson J, Benetazzo A (2019) Maximum wave heights from global model reanalysis. Prog Oceanogr 175:139–160. https://doi.org/10.1016/j.pocean.2019.03.009

Belmonte Rivas M, Stoffelen A (2019) Characterizing ERA-Interim and ERA5 surface wind biases using ASCAT. Ocean Sci 15:831–852. https://doi.org/10.5194/os-15-831-2019

Bidlot J (2010) Use of MERCATOR surface currents in the ECMWF forecasting system. ECMWF Research Department Memorandum. Reading, United Kingdom. R60.9/JB/1

Bidlot J-R (2012a) Present status of wave forecasting at ECMWF. In: Workshop on Ocean Waves. ECMWF, Reading, United Kingdom

Bidlot J (2012b) Use of MERCATOR surface currents in the ECMWF forecasting system: a follow-up study. ECMWF Research Department Memorandum. Reading, United Kingdom

Bidlot J, Janssen P, Abdalla S (2007) A revised formulation of ocean wave dissipation and its model impact ECMWF. Tech. Memo. 509. ECMWF, Reading, United Kingdom, 27pp. Available online at: http://www.ecmwf.int/publications/. 29

Caires S, Sterl A, Bidlot JR, Graham N, Swail V (2004) Intercomparison of different wind-wave reanalyses. J Clim 17:1893–1913. https://doi.org/10.1175/1520-0442(2004)017<1893:IODWR>2.0.CO;2

Cavaleri L, Bertotti L, Torrisi L, Bitner-Gregersen E, Serio M, Onorato M (2012) Rogue waves in crossing seas: the Louis Majesty accident. J Geophys Res Ocean 117. https://doi.org/10.1029/2012JC007923

Chatelain M, Guizien K (2010) Modelling coupled turbulence-dissolved oxygen dynamics near the sediment-water interface under wind waves and sea swell. Water Res 44:1361–1372. https://doi.org/10.1016/j.watres.2009.11.010

Chawla A, Spindler DM, Tolman HL (2013) Validation of a thirty year wave hindcast using the Climate Forecast System Reanalysis winds-12th International Workshop on Wave Hindcasting and Forecasting. Ocean Model 70:189–206. https://doi.org/10.1016/j.ocemod.2012.07.005

Dee DP, Uppala SM, Simmons AJ, Berrisford P, Poli P, Kobayashi S, Andrae U, Balmaseda MA, Balsamo G, Bauer P, Bechtold P, Beljaars ACM, van de Berg L, Bidlot J, Bormann N, Delsol C, Dragani R, Fuentes M, Geer AJ, Haimberger L, Healy SB, Hersbach H, Hólm EV, Isaksen L, Kållberg P, Köhler M, Matricardi M, McNally AP, Monge-Sanz BM, Morcrette JJ, Park BK, Peubey C, de Rosnay P, Tavolato C, Thépaut JN, Vitart F (2011) The ERA-Interim reanalysis: configuration and performance of the data assimilation system. Q J R Meteorol Soc 137:553–597. https://doi.org/10.1002/qj.828

Drévillon M, Régnier C, Lellouche J-M, et al (2018) CMEMS Quality Information Document for Global Ocean Reanalysis Products-GLOBAL-REANALYSIS-PHY-001-030. 1–48

Durrant TH, Greenslade DJM, Simmonds I (2013) The effect of statistical wind corrections on global wave forecasts. Ocean Model 70:116–131. https://doi.org/10.1016/j.ocemod.2012.10.006

ECMWF (2012) IFS DOCUMENTATION–Part VII: ECMWF Wave Model. IFS Doc CY41R1 1–79

Gallet B, Young WR (2014) Refraction of swell by surface currents. J Mar Res 72:105–126. https://doi.org/10.1357/002224014813758959

Gunn K, Stock-Williams C (2012) Quantifying the global wave power resource. Renew Energy 44:296–304. https://doi.org/10.1016/j.renene.2012.01.101

Hajduch G, Vincent P, Meadows P, Small D (2020) Sentinel 1 Annual Performance Report for 2019, version 1.1. https://doi.org/10.13140/RG.2.2.28472.16646

Hasselmann S, Hasselmann K (1985) Computations and parameterizations of the nonlinear energy transfer in a gravity-wave spectrum. Part I: a new method for efficient computations of the exact nonlinear transfer integral. J Phys Ocean 15:1369–1377. https://doi.org/10.1175/1520-0485(1985)015<1369:capotn>2.0.co;2

Hasselmann K, Hasselmann S, Bauer E et al (1988) The WAM model-a third generation ocean wave prediction model. J Phys Ocean 18:1775–1810

Hasselmann K, Chapron B, Aouf L et al (2013) The ERS SAR wave mode: a breakthrough in global ocean wave observations. In: European Space Agency, (Special Publication) ESA SP, pp 167–197

Hersbach H, Bell B, Berrisford P, Hirahara S, Horányi A, Muñoz-Sabater J, Nicolas J, Peubey C, Radu R, Schepers D, Simmons A, Soci C, Abdalla S, Abellan X, Balsamo G, Bechtold P, Biavati G, Bidlot J, Bonavita M, Chiara G, Dahlgren P, Dee D, Diamantakis M, Dragani R, Flemming J, Forbes R, Fuentes M, Geer A, Haimberger L, Healy S, Hogan RJ, Hólm E, Janisková M, Keeley S, Laloyaux P, Lopez P, Lupu C, Radnoti G, Rosnay P, Rozum I, Vamborg F, Villaume S, Thépaut JN (2020) The ERA5 global reanalysis. Q J R Meteorol Soc 146:1999–2049. https://doi.org/10.1002/qj.3803

Irvine DE, Tilley DG (1988) Ocean wave directional spectra and wave-current interaction in the Agulhas from the shuttle imaging radar-B synthetic aperture radar. J Geophys Res Ocean 93:15389–15401. https://doi.org/10.1029/JC093iC12p15389

Knapp KR, Kruk MC, Levinson DH, Diamond HJ, Neumann CJ (2010) The international best track archive for climate stewardship (IBTrACS). Bull Am Meteorol Soc 91:363–376. https://doi.org/10.1175/2009BAMS2755.1

Kobayashi S, Ota Y, Harada Y et al (2015) The JRA-55 reanalysis: general specifications and basic characteristics. J Meteorol Soc Japan 93:5–48. https://doi.org/10.2151/jmsj.2015-001

Law-Chune S, Aouf L, Bruno L, Dalphinet A (2019) CMEMS Quality Information Document for GLOBAL Ocean Waves Reanalysis GLOBAL_REANALYSIS_WAV_001_032

Le Traon PY, Reppucci A, Alvarez Fanjul E et al (2019) From observation to information and users: the Copernicus Marine Service perspective. Front Mar Sci 6. https://doi.org/10.3389/fmars.2019.00234

Lellouche J-M, Greiner E, Le Galloudec O et al (2018) Recent updates on the Copernicus Marine Service global ocean monitoring and forecasting real-time 1/12° high resolution system. Ocean Sci Discuss:1–70. https://doi.org/10.5194/os-2018-15

Lemos G, Semedo A, Dobrynin M, Behrens A, Staneva J, Bidlot JR, Miranda PMA (2019) Mid-twenty-first century global wave climate projections: results from a dynamic CMIP5 based ensemble. Glob Planet Change 172:69–87. https://doi.org/10.1016/j.gloplacha.2018.09.011

Li H, Yu C, Chen R, Li J, Li J (2012) Novel ionic liquid-type Gemini surfactants: synthesis, surface property and antimicrobial activity. Colloids Surfaces A Physicochem Eng Asp 395:116–124. https://doi.org/10.1016/j.colsurfa.2011.12.014

Lionello P, Gunther H, Janssen PAEM (1992) Assimilation of altimeter data in a global third-generation wave model. J Geophys Res 97:14453. https://doi.org/10.1029/92jc01055

Mapp GR, Welch CS, Munday JC (1985) Wave refraction by warm core rings. J Geophys Res 90:7153. https://doi.org/10.1029/jc090ic04p07153

Mazas F, Hamm L (2011) A multi-distribution approach to POT methods for determining extreme wave heights. Coast Eng 58:385–394. https://doi.org/10.1016/j.coastaleng.2010.12.003

Mentaschi L, Besio G, Cassola F, Mazzino A (2013) Problems in RMSE-based wave model validations. Ocean Model 72:53–58. https://doi.org/10.1016/j.ocemod.2013.08.003

Mínguez R, Reguero BG, Luceño A, Méndez FJ (2012) Regression models for outlier identification (hurricanes and typhoons) in wave hindcast databases. J Atmos Ocean Technol 29:267–285. https://doi.org/10.1175/JTECH-D-11-00059.1

Mori N, Shimura T, Kamahori H, Chawla A (2017) Historical wave climate hindcasts based on Jra-55. Proc Coast Dyn

National Geophysical Data Center N (2006) National Geophysical Data Center, 2006. 2-minute Gridded Global Relief Data (ETOPO2) v2. In: Natl. Geophys. Data Center, NOAA

Perez J, Menendez M, Losada IJ (2017) GOW2: a global wave hindcast for coastal applications. Coast Eng 124:1–11. https://doi.org/10.1016/j.coastaleng.2017.03.005

Queffeulou P, Croizé-Fillon D (2016) Global altimeter SWH data set–September 2016. IFremer, Plouzane, France

Roh M-I (2013) Determination of an economical shipping route considering the effects of sea state for lower fuel consumption. Int J Nav Archit Ocean Eng 5:246–262. https://doi.org/10.2478/ijnaoe-2013-0130

Röhrs J, Christensen KH, Vikebø F, Sundby S, Saetra Ø, Broström G (2014) Wave-induced transport and vertical mixing of pelagic eggs and larvae. Limnol Oceanogr 59:1213–1227. https://doi.org/10.4319/lo.2014.59.4.1213

Saha S, Moorthi S, Pan HL, Wu X, Wang J, Nadiga S, Tripp P, Kistler R, Woollen J, Behringer D, Liu H, Stokes D, Grumbine R, Gayno G, Wang J, Hou YT, Chuang HY, Juang HMH, Sela J, Iredell M, Treadon R, Kleist D, van Delst P, Keyser D, Derber J, Ek M, Meng J, Wei H, Yang R, Lord S, van den Dool H, Kumar A, Wang W, Long C, Chelliah M, Xue Y, Huang B, Schemm JK, Ebisuzaki W, Lin R, Xie P, Chen M, Zhou S, Higgins W, Zou CZ, Liu Q, Chen Y, Han Y, Cucurull L, Reynolds RW, Rutledge G, Goldberg M (2010) The NCEP climate forecast system reanalysis. Bull Am Meteorol Soc 91:1015–1057. https://doi.org/10.1175/2010BAMS3001.1

Sarpkaya TS (2012) Wave forces on offshore structures. In: Cambridge University (ed) Wave forces on offshore structures. pp 285–320. https://doi.org/10.1017/CBO9781139195898.009doi:10.1017/CBO9781139195898.009

Stopa JE (2018) Wind forcing calibration and wave hindcast comparison using multiple reanalysis and merged satellite wind datasets. Ocean Model 127:55–69. https://doi.org/10.1016/j.ocemod.2018.04.008

Szelangiewicz T, Wisniewski B, Zelazny K (2014) The influence of wind, wave and loading condition on total resistance and speed of the vessel. Polish Marit Res 21:61–67. https://doi.org/10.2478/pomr-2014-0031

Timmermans BW, Gommenginger CP, Dodet G, Bidlot JR (2020) Global wave height trends and variability from new multimission satellite altimeter products, reanalyses, and wave buoys. Geophys Res Lett 47. https://doi.org/10.1029/2019GL086880

Uppala SM, Kållberg PW, Simmons AJ et al (2005) The ERA-40 re-analysis. Q J R Meteorol Soc 131:2961–3012

Vinet L, Zhedanov A (2011) A "missing" family of classical orthogonal polynomials. J Phys A Math Theor 44:98–106. https://doi.org/10.1088/1751-8113/44/8/085201

Young IR (2017) A review of parametric descriptions of tropical cyclone wind-wave generation. Atmosphere (Basel) 8. https://doi.org/10.3390/atmos8100194